Polycomb proteins control floral determinacy by H3K27me3-mediated repression of pluripotency genes in arabidopsis thaliana

Polycomb Proteins Control Floral Determinacy by H3K27me3-mediated Repression of Pluripotency Genes in *Arabidopsis thaliana*

Ralf Müller-Xing[1,2,3,4¶*], Rhomi Ardiansyah[1,2,3¶], Qian Xing[1,2,3¶*], Léa Faivre[5¶], Jingjing Tian[2,3¶], Guohua Wang[6,7], Yucai Zheng[1,2,3], Xue Wang[3], Tingting Jing[1,2,3], Erica de Leau[4], Song Chen[6], Su Chen[6], Daniel Schubert[5], and Justin Goodrich[4]

[1] Plant Epigenetics and Development, Lushan Botanical Garden, Jiangxi Province and Chinese Academy of Sciences, Nanchang, China

[2] Key Laboratory of Saline-Alkali Vegetation Ecology Restoration (Northeast Forestry University), Ministry of Education, Harbin, China

[3] Plant Epigenetics and Development, Institute of Genetics, College of Life Science, Northeast Forestry University, Harbin, China

[4] Institute of Molecular Plant Sciences, The University of Edinburgh, Edinburgh, United Kingdom

[5] Epigenetics of Plants, Freie Universität Berlin, Berlin, Germany

[6] State Key Laboratory of Tree Genetics and Breeding, Northeast Forestry University, Harbin, Heilongjiang, China

[7] Information and Computer Engineering College, Northeast Forestry University, Harbin, Heilongjiang, China

* Corresponding authors:
Ralf Müller-Xing (Ralf.Mueller@hhu.de) and Qian Xing (qxing@lsbg.cn)

¶ These authors contributed equally to this work.

Keywords: Flower development, epigenetic gene regulation, PcG proteins, floral stem cell determinacy, MADS box genes, floral organ specification

Highlight

Polycomb proteins promote flower development and determinacy at multi-levels of the floral gene regulatory network by silencing direct targets including floral regulators like *AGL24* and pluripotency genes such as *STM*.

Abstract

Polycomb group (PcG) protein-mediated histone methylation (H3K27me3) controls the correct spatiotemporal expression of numerous developmental regulators in Arabidopsis. Epigenetic silencing of the stem cell factor *WUS* in floral meristems (FMs) depends on H3K27me3 deposition by PcG proteins. However, the role of H3K27me3 in silencing of other meristematic regulator and pluripotency genes during FM determinacy has not yet been studied. To this end, we report the genome-wide dynamics of H3K27me3 levels during FM arrest and the consequences of strongly depleted PcG activity on early flower morphogenesis including enlarged and indeterminate FMs. Strong depletion of H3K27me3 levels results in misexpression of the FM identity gene *AGL24*, which partially leads to floral reversion causing *ap1*-like flowers and indeterminate FMs expressing ectopically *WUS* and *STM*. Loss of *STM* can rescue supernumerary floral organs and FM indeterminacy in H3K27me3-deficient flowers indicating that the hyperactivity of the FMs is at least partially a result of ectopic *STM* expression. Nonetheless, *WUS* remained essential for the FM activity. Our results demonstrate that PcG proteins promote FM determinacy at multi-levels of the floral gene regulatory network, silencing initially floral regulators like *AGL24* that promotes FM indeterminacy, and subsequently, meristematic pluripotency genes such as *WUS* and *STM* during FM arrest.

Introduction

In plants, the epigenetic machinery provides stable gene expression patterns, which enable the formation of various tissues and whole organs including roots, shoots and flowers (Xiao et al., 2017; Jing et al., 2020). All aerial parts of plants are formed from the shoot apical meristem (SAM) (Nägeli, 1858) carrying a self-maintaining stem cell pool that enables lifelong organogenesis (Williams and Fletcher, 2005; Soyars et al., 2016). The homeostasis of this stem cell niche depends on a negative feed-back loop in *Arabidopsis thaliana* (Arabidopsis): The transcription factor (TF) WUSCHEL (WUS) is expressed in cells of the organizing center (OC) directly underneath the stem cells. Intercellular movement of WUS from the OC to the stem cells at the top of the SAM is required for non-cell autonomous maintenance of the stem cells and activates the stem cell-specific *CLAVATA 3* (*CLV3*) gene encoding a small secreted signal peptide (Fletcher et al., 1999; Schoof et al., 2000; Yadav et al., 2011; Daum et al., 2014). In turn, the CLV3 peptide is perceived by receptor kinases including CLAVATA 1 (CLV1) and CLV2-CORYNE (CRN) in the underlying cells of the OC to dampen *WUS* expression (Brand et al., 2000; Müller et al., 2006; Müller et al., 2008). In this feedback loop, WUS promotes stem cell fate and *CLV3* expression, while CLV3 represses *WUS*. This feedback regulation maintains the size of OC and stem cell niche and, ultimately, the size and function of the SAM (Somssich et al., 2016). Furthermore, several members of the homeodomain (HD) TF superfamily play a vital role in determining meristem functions including the BEL1-like (BELL) members PENNYWISE (PNY) and POUNDFOOLISH (PNF) and the four members of the KNOX/KNAT (for KNOTTED-like from *Arabidopsis thaliana*) class I, SHOOT MERISTEMLESS (STM), BREVIPEDICELLUS (BP)/KNAT1, KNAT2, and KNAT6 (Scofield and Murray, 2006).

After transition from the vegetative to the reproductive phase, the SAM converts into an inflorescence meristem (IM) producing flowers at its flanks. The floral meristems (FMs) generate primordia of the flower organs which are organized in four whorls: four sepals in whorl 1, four petals in whorl 2, six stamens in whorl 3 and two fused carpels in whorl 4 (Alvarez-Buylla et al., 2010). Antagonistic interaction between the IM identity genes *TERMINAL FLOWER 1* (*TFL1*) and *AGAMOUS-LIKE 24* (*AGL24*) and the FM identity genes, *LEAFY* (*LFY*), *APETALA 1* (*AP1*) and *CAULIFLOWER* (*CAL*) maintains the identity of both types of SAMs (Bradley et al., 1997; Liljegren et al., 1999; Ratcliffe et al., 1999). *AP1* and *CAL* encode MADS domain TFs that have partially redundant activities involved in the formation of FMs by repression of *TFL1* (Ratcliffe et al., 1999; Kempin et al., 1995). In turn, *TFL1* bars *AP1* and *LFY* expression in IMs (Liljegren et al., 1999; Ratcliffe et al., 1999). *LFY* encodes a plant specific TF that activates *AP1* but also *TFL1* expression

suggesting that *LFY* and *AP1/CAL* have partially antagonistic activities in the control of floral initiation (Serrano-Mislata et al., 2017; Goslin et al., 2017).

The ABC model describes how a few genes act together to specify the four types of flower organs (Coen and Meyerowitz, 1991; Causier et al., 2010): Sepals are specified by A-function genes, petals by a combination of A and B-function genes, stamens by genes of B and C-function, and C-function alone specifies carpels. LFY activates the expression of the ABC-type MADS domain TFs AP1 (class A), APETALA 3 and PISTILLATA (AP3 and PI; both class B), and AGAMOUS (AG; class C) that also terminates *WUS* expression in FMs (Causier et al., 2010). The molecular basis of floral organ identity specification is the combinatorial formation of tetrameric complexes between the ABC-type MADS domain TFs with the E function MADS domain TFs, SEPALLATA 1-4 (SEP1-4) (Ditta et al., 2004; Melzer et al., 2009; Pelaz et al., 2000).

FM specification requires also the downregulation of the MADS box and flowering time genes *FRUITFULL* (*FUL*), *SUPPRESSOR OF OVEREXPRESSION OF CONSTANS 1* (*SOC1*), *SHORT VEGETATIVE PHASE* (*SVP*), and *AGL24* by direct binding of AP1 (Alvarez-Buylla et al., 2010; Yu et al., 2004; Liu et al., 2007; Chu et al., 2010; Kaufmann et al., 2010). Overexpression of *AGL24* causes FMs to revert to IMs phenocopying *ap1* mutant flowers with secondary flowers in the axils of leaf-like sepals (Yu et al., 2004; Liu et al., 2007). During the stage 1 and 2 of flower development, AGL24 and SVP form dimers with AP1 to repress directly the class B, C and E floral homeotic genes *AP3*, *PI*, *AG* and *SEP3* (Gregis et al., 2006; Gregis et al., 2009; Liu et al., 2009). *AGL24* and *SVP* are also FM identity genes since the *ap1 svp agl24* triple mutant continuously produces IMs in place of flowers (Gregis et al., 2008). Furthermore, AGL24 acts redundantly with SOC1, SVP, and SEP4 directly suppressing *TFL1* in emerging FMs, which prevents floral reversion (Liu et al., 2013). These findings indicate that *AGL24* has features of an IM as well as a FM identity gene.

All above mentioned TFs are targets of the epigenetic repressive mark H3K27me3 (tri-methylation of Lys-27 on histone H3), which is associated with Polycomb (PcG) function (Zhang et al., 2007; Lafos et al., 2011). The SET domain-containing histone methyltransferase (HMT) Enhancer of zeste (E(z)), which is the catalytic subunit of the Polycomb Repressive Complex 2 (PRC2), silences PcG target genes by H3K27me3 (Schuettengruber et al., 2017). In Arabidopsis, E(z) is encoded by three homologs including *CURLY LEAF* (*CLF*) and *SWINGER* (*SWN*) (Spillane et al., 2000; Mozgova and Hennig, 2015). One further core component of PRC2 is Suppressor of zeste 12 (Su(z)12), which is encoded by three homologs including *EMBRYONIC FLOWER 2* (*EMF2*), and *VERNALIZATION 2* (*VRN2*) in Arabidopsis (Chanvivattana et al., 2004). Like *CLF* and *SWN*, *EMF2* and *VRN2* are essential for the

postembryonic development since severe *emf2-3 vrn2-1* and *clf swn* mutant seedlings form only callus-like tissue after germination (Schubert et al., 2005). Recently, we introduced two plant lines with strongly depleted PcG activity, *clf-28 swn-7 CLF-GR* (*iCLF*) and *emf2-10 vrn2-1* double mutants, which form leaves and shoots bearing flowers with diverse defects, although global H3K27me3 levels are highly reduced (Lafos et al., 2011; Müller-Xing et al., 2014; Müller-Xing et al., 2015).

Normal flower development requires both, initiation and termination of the floral stem cell niche by the balance between the positive stem cell factor WUS and the negative regulator AG, which form a positive–negative feedback loop (Lenhard et al., 2001; Lohmann et al., 2001; Ming and Ma, 2009). After initiating in stage 2, WUS activates together with LFY the expression of *AG*. In turn, AG represses *WUS* expression that fully vanishes during floral stage 6, followed by loss of the floral stem cell pool (Lenhard et al., 2001; Lohmann et al., 2001). The silencing of *WUS* is accompanied by direct recruitment of PRC2, and subsequently, H3K27me3 deposition at the *WUS* chromatin (Liu et al., 2011; Sun et al., 2019). Nevertheless, the significance of H3K27me3 deposition for gene silencing of other meristematic genes during termination of the floral stem cell population, remained largely unclear.

In our study, we explored the impact of cumulative H3K27me3 levels on early flower morphogenesis using a combined approach of mutant analyses and genome-wide profiling of H3K27me3. Strongly depleted PcG activity results in enlarged and indeterminate FMs consistent with increased and prolonged stem cell activity. Surprisingly, we found evidences that this hyperactivity of the FMs is partially independent of *WUS* expression levels giving rise to the possibility that PcG proteins control FM size and determinacy also through silencing of other meristematic regulators. We identified candidates by genome-wide H3K27me3 profiling during FM arrest, and subsequently, expression analysis in PcG mutants. Based on our double mutant and gene expression studies, we propose that the H3K27me3-mediated silencing of *AGL24* and *STM* is of similar importance as silencing of *WUS* for the control of FM determinacy by PcG proteins.

Materials and Methods

Plant Materials and Growth Conditions

Arabidopsis (*Arabidopsis thaliana* (L.) Heynh.) plants were grown at 21°C under long-day (16 h light/8 h dark) conditions, unless indicated otherwise. *iCLF* (*clf-28 swn-7 CLFpro:CLF-GR*, in Col-0 background), *emf2-10 vrn2-1* (Ws-0), and *emf2-10 vrn2-1* backcrossed to La-0 were described previously (Lafos et al., 2011; Müller-Xing et al., 2014; Müller-Xing et al., 2015). *emf2-10 vrn2-1* (La-0) was backcrossed to L*er*-0 to generate *emf2-10 vrn2-1 erecta* (*ev er*) to obtain an Arabidopsis line with strongly depleted PcG activity in *er* mutant background. In each experiment, the corresponding ecotype was used as wild-type control. *agl24-1* mutants (Michaels et al., 2003) and *STM::GUS* (Kirch et al., 2003) were kindly provided by R.M. Amasino and Wolfgang Werr, respectively. *clf-28 swn-7*, *clv1-11, clv3-2, crn-1*, *wus-1*, *WUS::GUS*, and *LEAFY::GUS* were previously described (Laux et al., 1996; Blázquez et al., 1997; Fletcher et al., 1999; Gross-Hardt et al., 2002; Diévart et al., 2003; Schubert et al., 2005; Müller et al., 2008). *ap1-1* (Irish and Sussex, 1990) was obtained from the Nottingham Arabidopsis Stock Centre. The *35S::AP1-GR ap1-1 cal-1* line (Wellmer et al., 2006), were kindly provided by Frank Wellmer and Yuling Jiao. After three weeks short-day (8 h light/16 h dark), the *35S::AP1-GR ap1-1 cal-1* plants were shifted to long-day and, five days later, induced with dexamethasone. We crossed *clv1-11, crn-1, clv3-2, wus-1, ap1-1, agl24-1*, and *bum1-3* to *emf2-10 vrn2-1* and/or *iCLF*, to generate triple mutants. Furthermore, we generated *emf2-10 vrn2-1* lines with *STM::GUS, WUS::GUS*, and *LEAFY::GUS* reporter genes.

RNA Extraction and RT-qPCR Analysis

For RT-qPCR analysis, inflorescences were dissected and open flowers (older than stage 12) were removed (Smyth et al., 1990). For harvesting of *35S::AP1-GR ap1-1 cal-1* samples, only the cauliflower structures of the main inflorescence were harvested. Leaf and pedicel tissue contamination was minimized by dissection as previously described (Engelhorn et al., 2017). Samples were collected from non-induced *35S::AP1-GR ap1-1 cal-1* (t0) tissue and *35S::AP1-GR ap1-1 cal-1* five days after induction (t5, ~ floral stage 7) (Wellmer et al., 2006; Smyth et al., 1990). Total RNA of three to six biological replicates was extracted with TRIZOL (Invitrogen) and cDNA was synthesized using RevertAid reverse transcriptase (Thermo Fisher). Real-time RT-qPCR was performed by using SYBR Green I for LightCycler 480 (Roche). As internal control served *eIF4A* since its expression is unchanged during early flower development or in PcG mutants if normalized to the *TIP41*, *RTFbox*

(*AT5G15710*), or *UBQ10* (**Supplementary Fig. S1**; (Wellmer et al., 2006; Li et al., 2020; Yan et al., 2020; Krizek et al., 2021; Di Sun et al., 2021). The expression levels are expressed as the mean of relative fold changes of at least three biological replicates (values are scaled to wild-type or t0), and the error bars represent the standard error of the mean (Student's *t* test); for N ≥ 4, the trimmed mean is shown. The RT-qPCR primers used are listed in S1 Table.

RNA *In Situ* Hybridization

Non-radioactive *in situ* hybridizations with *CLV3*, *WUS*, *STM*, *AP3* and *LFY* antisense probes were performed as previously described (Müller-Xing et al., 2014). The *SVP* plasmid for generating antisense probes was kindly provided by Peter Huijser (Hartmann et al., 2000).

Chromatin immunoprecipitation (ChIP) Assay and ChIP-Seq

ChIP assays were performed as described previously (Müller-Xing et al., 2014). The chromatin was fragmented to an average length of 200-400bp by sonication. We used the anti-tri-methylated histone H3K27 antibody (Abcam; ab6002). DNA was recovered by Phenol:chloroform:Isoamyl Alcohol (25:24:1). Then, the DNA was analyzed by ChIP-qPCR, the primers used are listed in S2 Table. For ChIP-Seq analysis the recovered DNA from the H3K27me3 ChIP experiment was combined in two biological replicas for each stage (*35S::AP1-GR ap1-1 cal-1*, t0 and t5). The ChIP-Seq assay were performed as described previously (Velanis et al., 2016) and were carried out in Glasgow Polyomics Facility (University of Glasgow).

ChIP-Seq Analysis

The H3K27me3 ChIP-Seq reads were aligned to the *Arabidopsis thaliana* genome, TAIR10 using Bowtie2 with default parameters. Multi-mapping reads and PCR duplicates were discarded together with unmapped reads, leaving only unique mapped reads for the downstream analysis. In order to retrieve the histone modifications patterns, peak calling was performed using MACS2 with the broad option and a p-value threshold set to 0.01 (Gaspar, 2018). The differential methylation analysis was ran using DiffBind with the DESeq2 method (p-value < 0.05) (Stark and Brown, 2011). The differentially methylated regions were assigned to genes using the ChIPseeker package (Yu et al., 2015). All those steps were performed using Curta, the High Performance Computing (HPC) of the

Freie Universität Berlin (Bennett et al., 2020). For each gene containing at least one differentially methylated region, a fold change was computed by counting the RPKM (Reads Per Kilobase and Million Mapped Reads) over the whole gene region (TSS to TES) in each condition using the featureCounts package and the RPKM function from edgeR (Liao et al., 2014). The Spearman correlation analysis was performed in R Studio using the expression data from Ryan et al., 2015. All steps until the R part of the analysis were performed using Curta; the computing time was kindly provided by the HPC Service of ZEDAT, Freie Universität Berlin. In addition, Venny 2.1 (https://bioinfogp.cnb.csic.es/tools/venny/index.html) was used for comparisons of gene lists and Integrative Genomic Viewer (IGV; Version2.3.88) was used for visualizing H3K27me3 pattern at gene loci to different time points.

GUS Staining

Detection of GUS activity in tissue preparations were performed as described with minor modifications (Li et al., 2020). In brief, inflorescences with flowers were harvested and immersed into the GUS Assay Solution (50 mM NaHPO4, 0.5 mM ferrocyanide, 0.5 mM ferricyanide, and 1% Triton X-100, pH 7.2) containing 1 mM X-Gluc. The tissues in the GUS solution were vacuum infiltrated for 30 min, and then incubated at 37°C for about 3 h to overnight. To remove the chlorophyll, stained tissues were carried through ethanol series and then observed with Nikon SMZ25 stereomicroscope.

Imaging

Photographs were taken either with a digital camera (Nikon D7200, Japan) or dissecting microscope with a 5 Mega Pixel digital camera (Motic K-500L, China). Digital photographs and graphics were collated with PowerPoint or Adobe Photoshop and adjusted as described before (Müller-Xing et al., 2014).

Results

Flowers with strong depletion of PcG activity feature increased size and indeterminacy of the floral meristems

In previous studies, we reported floral reversion in Arabidopsis lines with strongly depleted PcG activity, such as *emf2-10 vrn2-1* or *iCLF* when shifted from inductive to noninductive conditions, demonstrating that H3K27me3 is required to maintain floral commitment and IM identity (Müller-Xing et al., 2014; Müller-Xing et al., 2015). Flowers of *emf2-10 vrn2-1* and *iCLF* display diverse but similar developmental defects during flower development indicating misregulation of a similar set of target genes (Müller-Xing et al., 2014). The features of flowers with strongly depleted PcG activity include with a low penetrance homeotic organ transformation and fused floral organs (**Fig. 1D-L**) and **Supplementary Fig. S2**). In contrast, additional floral organs are the predominant phenotype of *emf2-10 vrn2-1* and *iCLF* flowers (**Fig. 1A-F** and **Supplementary Fig. S2**). The number of all floral organ types was increased with the exception of stamens (**Fig. 1I** and **Supplementary Fig. S2F**). Supernumerary floral organs often are the result of an increased FM size (Müller et al., 2008). Therefore, we measured the diameter of *emf2-10 vrn2-1* mutant FMs in longitudinal sections of floral primordia, stage 3-4. Like vegetative SAM and IM (**Fig. 2A-D**), the FM size was significantly increased in *emf2-10 vrn2-1*, while the FM domes were rather higher than wider in comparison to wild-type (**Supplementary Fig. S3**). Thus, the extra carpels in flowers with strongly depleted PcG activity could be caused by the enlarged FMs.

The carpels of *emf2-10 vrn2-1* and *iCLF* flowers were normally fused to form a club-shaped silique (**Fig. 1D,K-M**). A small proportion of the siliques displayed incomplete valve fusion at their distal ends, which opened the view to a fifth whorl that was composed of ectopic carpels (**Supplementary Fig. S2H**). To test the frequency of fifth whorls in *emf2-10 vrn2-1* and *iCLF* flowers, we opened siliques with fused carpels (**Fig. 1M**) and found that 70 to 90 percent of the siliques contained a fifth whorl. Also, *clv* and *crn* mutants develop enlarged and indeterminate FMs causing club-shaped siliques with increased numbers of carpels and a fifth whorl (Clark et al., 1993; 1995; Kayes and Clark, 1998; Müller et al., 2008) resembling siliques with strongly depleted PcG activity (**Supplementary Figs S4** and **S5**). Similar to *emf2-10 vrn2-1* and *iCLF*, *clv2* mutants exhibit flower-to-shoot transformation specifically under SD growth conditions (Kayes and Clark, 1998; Müller-Xing et al., 2014; Müller-Xing et al., 2015). Furthermore, the morphology of the gynoecia in *emf2-10 vrn2-1* and *iCLF* flowers were occasionally altered, and the portion covered by valves was reduced (**Supplementary Fig. S2D**).

This valveless phenotype is also associated with *clv* mutant siliques (Kayes and Clark, 1998; Diévart et al., 2003). To summarize, increased carpel number, enlarged and indeterminate FMs that produce a fifth whorl, club-shape and valveless siliques are phenotypes of flowers with strongly depleted PcG activity shared with *clv* mutants.

PcG activity promotes determinacy of the floral stem cell pool in parallel to *CLV3* signaling and partially independent of *WUS* expression levels

The enlarged size of vegetative SAM, IM and FMs and the similarity of the silique phenotype in plants with strongly depleted PcG activity to those of *clv* mutants suggest that *CLV3* signaling and PcG function might act in a common genetic pathway to suppress *WUS* expression. To test this hypothesis, we analyzed the expression patterns of *CLV3*, which is an established stem cell marker (Fletcher et al., 1999), and *WUS* in *emf2-10 vrn2-1* mutant flowers by RNA *in situ* hybridization and histochemical staining for *WUS::GUS* reporter gene activity (**Fig. 2E-L**). The *CLV3* expression domain appeared triangular in longitudinal sections of wild-type meristems. In the enlarged *emf2-10 vrn2-1* IMs and FMs, *CLV3* was stronger expressed in slightly expanded domains indicating accumulation of more floral stem cells. Furthermore, *CLV3* expression was also temporally extended and maintained beyond stage 6 of flower development, consistent with the hypothesis that increased and prolonged stem cell activity induces the formation of a fifth whorl (**Supplementary Fig. S5F**). Although *WUS* is also expressed beyond flower stage 6 (**Fig. 2K-L,P**), the *WUS* expression domain in *emf2-10 vrn2-1* IMs and FMs appeared smaller and the staining weaker (**Fig. 2G-H**), suggesting that weaker *WUS* is not the reason but the consequence of increased *CLV3* expression.

In order to determine whether the *clv*-like phenotype of flower with strongly depleted PcG activity might be due to lost or reduced activity of *CLV3* or of the CLV3 receptors, we combined *emf2-10 vrn2-1* with several *CLV3* signaling mutants. We examined the floral organ number in *clv3-2 emf2-10 vrn2-1* triple mutants and found that the carpel number was increased to 7.8 in comparison to 6.0 in *clv3-2* single mutants and 3.9 in *emf2-10 vrn2-1* double mutants (**Fig. 2M-O,Q**). Thus, *clv3-2* mutants strongly enhanced PcG double mutants indicating that *CLV3* signaling and PcG proteins restrict the number of carpels independently. Also, the valveless phenotype was enhanced in *clv3-2 emf2-10 vrn2-1* siliques (**Supplementary Fig. S4**). The analysis of *clv1-11 emf2-10 vrn2-1* and *crn-1 emf2-10 vrn2-1* triple mutants gave similar results (**Supplementary Fig. S5**). From this genetic analysis, we conclude

that *CLV3* signaling and PcG proteins restrict size and termination of FMs independently of one another.

We confirmed by RT-qPCRs that *CLV3* is upregulated in *emf2-10 vrn2-1* inflorescences and found synergistically enhanced *CLV3* expression (96.3x higher than wild-type) in *clv3-2 emf2-10 vrn2-1* triple mutants (**Fig. 2R**). This is in line with our carpel number analysis (**Fig. 2Q**), and the conclusion that *CLV3* signaling and PcG proteins control the floral stem cell population in parallel pathways. Similar to the stem cell marker *CLV3*, the meristem marker *STM* was upregulated in *emf2-10 vrn2-1* (**Fig. 2R**). Notably, loss of *CLV3* had no significant effect on *STM* expression either in PcG deficient or wild-type plants indicating that PcG activity but not *CLV3* signaling restricts *STM* expression. We also confirmed the downregulation of *WUS* in *emf2-10 vrn2-1* inflorescences (**Fig. 2R**). Thus, we reasoned that the increased *CLV3* expression could cause the lower *WUS* expression, but we found only a partial rescue of *WUS* in *clv3-2 emf2-10 vrn2-1* triple mutants (**Fig. 2R**) suggesting the upregulation of other *WUS* repressors in *emf2-10 vrn2-1*.

Our genetic analysis of flower phenotype and gene expression in *clv3-2 emf2-10 vrn2-1* triple mutants revealed that *CLV3* signaling and PcG proteins control the floral stem cell population in parallel pathways. Although *WUS* expression was temporally extended beyond floral stage 6 in PcG double mutants, *WUS* expression was lower in *emf2-10 vrn2-1* meristems. This finding suggests that the expansion of the stem cell domain is at least partially independent of *WUS* expression levels. It also gives rise to the possibility that PcG proteins control FM size and determinacy by repressing other meristematic regulators through H3K27me3 deposition.

Genome-wide analyses of changes in H3K27me3 levels after floral meristem determinacy

We reasoned that profiling of the dynamics of H3K27me3 accumulation rather than profiling the loss of H3K27me3 in unconditional PcG mutants could identify meristematic genes that are silenced by PcG proteins during early flower development. To investigate the dynamics of H3K27me3, we took advantage of the previously described *AP1-GR ap1-1 cal-1* floral induction system (Wellmer et al., 2006), which can provide synchronized flower tissue of specific developmental stages (**Fig. 3A-B)**. To assess the correlation of FM termination and changes of H3K27me3 levels, we chose floral primordia in stage 7 (t5, five days after induction with dexamethasone), which constitutes the earliest floral stage without meristematic tissue. We performed RT-qPCRs and ChIP-qPCRs to validate the t5 samples in comparison to the non-induced reference samples with IM tissue (t0). In wild-type inflorescences, *SVP*

mRNA accumulates in floral primordia at stage 1 and 2 and is silenced in floral primordia during stage 3 (**Fig 3C**). In the t5 samples, expression of the stem cell marker *CLV3* was reduced to background levels indicating the presence of only post-meristematic tissue, while *SVP* mRNA levels were decreased to less than three percent of the mRNA levels in the t0 samples, whereas *SVP* H3K27me3 levels tripled (**Supplementary Fig. S6**). These data suggested that the tissues of the *AP1-GR ap1-1 cal-1* t0 and t5 samples were homogenous and the t5 showed synchronized and uniform floral induction, so that we proceeded with the ChIP Seq approach.

In floral stage 7 (t5), we identified 466 differentially methylated peaks corresponding to 420 differentially methylated genes (DMG) including *SVP* (**Fig. 3D-F**). 296 coding genes, 3 microRNAs and 5 transposable elements significantly increased H3K27me3 levels in comparison to the controls (t0) (**Fig. 3D**). *OBO1* showed the highest increase in H3K27me3 levels (17.8-fold), while *OBO2* was the most heavily methylated H3K27me3 target gene at t5 (190.3 RPKM in **Table 1 and Supplementary Table S5**). On the other hand, chromatin loci of 110 coding genes, 1 microRNAs and 5 transposable elements had significantly decreased H3K27me3 levels in the t5 samples compared to the control (t0) samples (**Fig. 3D**). The strongest H3K27me3 reduction of all coding genes occurred at *SEP3* chromatin (**Supplementary Fig. S8A-B** and **Supplementary Table S6**), which encodes the most prominent E function co-factor for ABC-type MADS TFs (Melzer et al., 2009; Pelaz et al., 2001; Immink et al., 2009; Lopez-Vernaza et al., 2012; Hugouvieux et al., 2018). Although *WUS* and *AG* were not among the DMGs identified by the ChIP Seq, we confirmed by independent ChIP-qPCR experiments that the *WUS-AG* negative feedback loop was accompanied by reduced H3K27me3 levels at *AG*, whereas the *WUS* gene locus significantly gained H3K27me3 (**Supplementary Fig. S9)**.

We compared our H3K27me3 data sets with published expression data (Ryan et al., 2015). We found that changes of H3K27me3 and expression levels were highly negatively correlated (**Fig. 4A-C**). In further comparison, we identified 151 coding genes that significantly gained H3K27me3 and had decreased expression rates, whereas 49 loci lost H3K27me3 and increased expression accordingly (**Fig. 4D-E**, **Supplementary Fig. S10** and **Supplementary Table S5 and S6**). To verify our ChIP seq data and the published expression data, we performed ChIP- and RT-qPCRs for some TF genes of interest on independent *AP1-GR ap1-1 cal-1* t0 and t5 samples (**Supplementary Figs S8**). Notably, TFs were highly over-represented (40.4% and 26.5%) within the genes that showed a negative correlation between changes in gene expression and changes in H3K27me3 (**Fig. 4D-E**). The majority of the genes, which are targeted by these H3K27me3 regulated TFs, are not H3K27me3 targets (**Supplementary Fig. S11**). This suggests that regulation by H3K27me3 is part of an epigenetic switch,

which stabilizes the expression changes of rather a few hundred TFs that, in turn, control transcriptional changes of thousands of genes that are largely not H3K27me3 targets. Furthermore, the three microRNA genes MIR2111B, MIR319A and MIR165B gained H3K27me3 (**Fig. 3D** and **Supplementary Table S7**) indicating indirectly positive regulation of coding genes by H3K27me3-mediated repression of microRNA genes during early flower development (Lafos et al., 2011).

To determine whether TF genes could contribute to the floral indeterminacy and other phenotypes in flowers with strongly depleted PcG activity, we examined the expression and H3K27me3 levels of several TFs in *emf2-10 vrn2-1* mutant inflorescences using RT-qPCR and ChIP-qPCR. Independent of whether they had increased or decreased H3K27me3 levels during early flower development, the majority of the tested TF genes (93.3 percent) lost H3K27me3 in *emf2-10 vrn2-1* (**Supplementary Figs S12)**. Within the TF genes that gained H3K27me3 and decreased expression in *AP1-GR ap1-1 cal-1* (t5-t0), we identified eight HD (seven TALE and one WOX) and seven MADS TF genes (**Fig. 4F** and **Table 1)**. Surprisingly, only five of the eight HD and four of the seven MADS TFs were upregulated in the PcG double mutants, whereas one MADS and two HD TF genes were downregulated (**Supplementary Figs S13**). Thus, only 60 percent of the HD and MADS TF genes, whose H3K27me3 levels increased during early flower development, were upregulated in strongly PcG deficient flowers, while the downregulation of three TF genes indicates that PcG proteins can indirectly promote their expression.

PcG proteins promote FM identity and determinacy by silencing *AGL24* that encodes a repressor of ABCE function genes and *STM*

The FM identity genes *LFY* and *AP1* directly upregulate each other in a positive feedback loop, and control the expression of floral homeotic MADS box genes (Kaufmann et al., 2010; Wagner et al., 1999; Moyroud et al., 2011). As expected, we found *AP3* and *SEP3* within the 49 coding genes which significantly lost H3K27me3 and increased expression rates during early flower morphogenesis (**Supplementary Fig. 8A** and **Supplementary Table S6**). To determine if loss of PcG activity promotes the expression of ABCE-type MADS box genes we performed RT-qPCRs with *emf2-10 vrn2-1* inflorescence tips. Surprisingly, the expression of *AP1*, *AP3*, *PI*, *AG* and *SEP3* were significantly reduced (**Fig. 5A**). Lower expression of *LFY* could explain the reduced expression rates of its target genes, but *LFY* was more highly expressed (**Fig. 5A** and **Supplementary Fig. S14**). An

alternative possibility is that genes which encode repressors of the ABCE genes were upregulated by strong depletion of PcG activity.

During the onset of flower development, *TFL1*, which encodes a repressor of *AP1*, is excluded from emerging floral primordia (Liljegren et al., 1999; Ratcliffe et al., 1999). The *TFL1* gene locus significantly gains in two days (t2) H3K27me3 levels (Engelhorn et al., 2017), which developed to robust changes (t5; **Supplementary Fig. S8D-E**). Notably, also the *FD* locus, encoding a bZIP TF that interacts with TFL1 to promote IM fate, gained H3K27me3 (t5; **Table 1**). To test the significance of H3K27me3 accumulation, we performed RT-qPCRs and found *TFL1* strongly upregulated in *emf2-10 vrn2-1* inflorescences (**Fig. 5A**). Up to 15 percent of *emf2-10 vrn2-1* and *iCLF* flowers carry secondary flowers in the axils of leaf-like sepals (**Fig. 1G-H,L**), which is a phenotype firstly associated with *ap1* A-function mutant flowers indicating partially reversion of FMs to IMs (**Supplementary Fig. S15A-C**) (Coen and Meyerowitz, 1991; Irish and Sussex, 1990). Therefore, the *ap1*-like phenotype could be caused by reduction of *AP1* expression by increased *TFL1*. However, the phenotype of *ap1* mutant flowers also includes loss of most petals but *emf2-10 vrn2-1* and *iCLF* flowers carry rather more petals, although some *iCLF* flowers had less petals (**Fig. 1A-D,I** and **Supplementary Fig. S2B**). To determine to what extent the *ap1*-like phenotype in *emf2-10 vrn2-1* flowers is attributable to decreased levels of *AP1* mRNA, we generated *ap1-1 emf2-10 vrn2-1* triple mutants. The percentage of secondary flowers in the axis of first-whorl organs was significantly increased in *ap1-1 emf2-10 vrn2-1* mutant flower compared to *ap1-1* single mutants indicating at least one *AP1*-independent pathway (**Supplementary Fig. S15A-F**).

Overexpression of the AP1 downstream target *AGL24* causes *ap1*-like and indeterminate flowers (Yu et al., 2004), which we also observed in *emf2-10 vrn2-1* mutant flower (**Fig. 5B-D)**. And indeed, *AGL24* was the most upregulated gene of all key floral regulators that we tested in *emf2-10 vrn2-1* mutant inflorescences, whereas H3K27me3 levels were strongly reduced at the *AGL24* gene locus (**Fig. 5A** and **Supplementary Figs S12B** and **S16**). Although the expression of *TFL1* was increased in *ap1-1 emf2-10 vrn2-1* mutant inflorescences, the loss of *AP1* did not significantly enhance *AGL24* expression in the PcG double mutants suggesting that the strong upregulation of *AGL24* is rather a direct result of the loss of H3K27me3 at the *AGL24* locus than an indirect result of reduced *AP1* expression (**Supplementary Fig. S15G**). Furthermore, *AGL24* expression was also increased in *iCLF* inflorescences and *clf swn* callus-like tissue (**Supplementary Fig. S17**). These findings indicate that increased *AGL24* activity could cause ectopic secondary flowers and FM indeterminacy in flowers with strongly depleted PcG activity. To test this hypothesis, we generated *emf2-10 vrn2-1* lines

segregating *agl24-1*. We found full suppression of the *ap1*-like phenotype in homozygous *agl24-1 emf2-10 vrn2-1* flowers, whereas 2.9 percent of *agl24-1/+ emf2-10 vrn2-1* flowers and 7.8 percent of *emf2-10 vrn2-1* flowers carried at least one secondary flower (**Fig. 5F**). In contrast, the carpel number was not affected, while the percentage of flowers with a fifth whorl decreased in *agl24-1 emf2-10 vrn2-1* triple mutant flowers (**Fig. 5G-H**). These results suggest that *AGL24* misexpression is the main cause for *ap1*-like flowers and contributes to the fifth whorl but has no effect on FM size or carpel number in plants with strong depleted PcG activity. *AGL24*, *SOC1* and *SVP* redundantly prevent ectopic expression of *AP3*, *PI*, *AG*, and *SEP3* in floral anlagen in the IM and in emerging FMs before stage 3 (Gregis et al., 2006; Gregis et al., 2009; Liu et al., 2009). Hence, the strong upregulation of *AGL24* could be one of the key factors that are involved in the decrease of *AP1*, *AP3*, *PI*, *AG* and *SEP3* expression (**Fig. 5A**) and therefore the ABC-function related homeotic transformation in flowers with strongly depleted PcG activity. To obtain additional evidence for this conclusion, we examined the expression in the inflorescences of *emf2-10 vrn2-1* double and *agl24-1 emf2-10 vrn2-1* triple mutant plants using RT-qPCR (**Fig. 5I**). Consistent with the hypothesis that *AGL24* overexpression directly causes the downregulation of the MADS TFs, the expression of *AP1*, *PI*, *SEP3*, and their target *AGL15* was rescued to wild-type levels, whereas *AP3* and *AG*, but also upregulated TF genes such as *LFY* and *TFL1*, were unchanged. This indicates that *AGL24* misexpression causes the downregulation of a subset of the TF genes that are downregulated in PcG double mutant flowers. Surprisingly, *STM* expression was synergistically increased in *emf2-10 vrn2-1 agl24-1* triple mutants (**Fig. 5I**). Thus, although *AGL24* promotes FM indeterminacy (Yu et al., 2004), *AGL24* acts redundantly with PcG proteins to prevent *STM* misexpression.

PcG proteins control FM activity by restriction of *STM* expression

STM is a well-known pluripotency gene belonging to the group of HD TF genes that gained H3K27me3 during FM determinacy (**Table 1**). Like in *emf2-10 vrn2-1*, we found increased *STM* mRNA levels in *iCLF* inflorescences and *clf-28 swn-7* callus-like tissue (**Fig. 5A** and **Supplementary Fig. S17**). To determine the spatiotemporal expression patterns of *STM* in PcG double mutant flowers, we analyzed *STM* expression in *emf2-10 vrn2-1* by RNA *in situ* hybridization and histochemical staining for *STM::GUS* reporter gene activity (**Fig. 6A-D**). *STM* was more strongly expressed in *emf2-10 vrn2-1* floral primordia than in wild-type, and like *WUS*, temporally extended beyond floral stage 6. This finding suggests that the ectopic expression of *STM* in the indeterminate FMs contribute to the fifth

whorl in flowers with strongly depleted PcG activity. Furthermore, increased *STM* activity could cause the enlarged FMs and extra floral organ numbers in H3K27me3 deficient flowers. To test this hypothesis, we combined the strong *STM* allele *bum1-3* with *emf2-10 vrn2-1* and *iCLF* constructing two lines with strongly depleted *STM* and PcG activity (**Fig. 6I** and **Supplementary Fig. S18**). Loss of *STM* affects the four floral whorls differently. While the total number of flower organs was reduced and all carpels lost, *bum1-3* flowers also displayed homeotic transformations of petals. The increased number of sepals were nearly rescued to wild-type in *bum1-3 emf2-10 vrn2-1* and *bum1-3 iCLF* flowers suggesting that increased *STM* activity contributes to the enlarged FM in the early stages of flowers with strongly depleted PcG activity. Loss of *STM* also rescued the increased carpel number in the strongly H3K27me3-deficient flowers of *bum1-3 iCLF* and *bum1-3 emf2-10 vrn2-1* triple mutants. Importantly, neither *bum1-3 iCLF* nor *bum1-3 emf2-10 vrn2-1* triple mutant flowers carried any fifth whorl structures (**Supplementary Table S9**). Similarly, loss of *WUS* resulted in premature arrest of FM activity in *wus-1 emf2-10 vrn2-1* mutant flowers indicated by lack of most central floral organs (**Fig. 6J**). These findings indicate that *WUS* and *STM* activity are essential for FM indeterminacy in flowers with strongly depleted PcG activity.

Discussion

H3K27me3-mediated gene silencing by PcG proteins has been implicated in a wide variety of developmental processes in Arabidopsis, including leaf differentiation and termination of *WUS* during FM arrest (Lafos et al., 2011; Liu et al., 2011; Sun et al., 2019). However, the significance of increasing H3K27me3 levels for silencing of other developmental genes during floral organ morphogenesis and termination of the floral stem cell population remained widely unexplored. Here we reveal new insights to the function of PcG proteins that restrict expression of their direct targets and promote gene expression indirectly by repressing transcriptional repressors in the gene regulatory network of TFs that controls early flower development (**Fig. 7**).

PcG proteins indirectly activate floral regulator genes by silencing of their upstream repressors like *AGL24*

In multicellular eukaryotes, including plants, H3K27me3 plays a fundamental role in the epigenetic regulation of tissue-specific expression patterns, which silences its direct targets and promotes gene expression indirectly by repressing miRNA genes (Lafos et al., 2011; Shivram et al., 2019). Although it has been implicated that PcG proteins can indirectly activate their own expression during seed development (Baroux et al., 2006), we provide here genetic evidence that PcG proteins indirectly activate TF genes by silencing of upstream transcriptional repressors. One third of the tested HD and MADS TF genes, although they lost the repressive H3K27me3 mark, were downregulated in *emf2-10 vrn2-1* double mutants. Particularly, the downregulation of ABCE-type MADS genes indicates that PcG proteins can indirectly promote gene expression. Within the MADS TF genes that showed the expected expression increase, we found *AGL24* mRNAs strongly accumulated. Several AGL24 target genes are known. On the onset of flower development, AGL24 acts redundantly with SVP, SOC1 and SEP4 to repress the expression of *TFL1*, while AGL24 forms with AP1 hetero-dimers that, redundantly with SVP-AP1 dimers, directly prevent premature expression of BCE-type MADS TF genes (Gregis et al., 2006; Gregis et al., 2009; Liu et al., 2013). Furthermore, SVP and AGL24 are direct positive regulators of *LFY* and *AP1* in FMs (Grandi et al., 2012). Although we could not confirm all of these transcriptional relations in strongly PcG-deficient background, we found correlation between ectopic *AGL24* activity and decreased expression of *PI*, *SEP3* and *AGL15*, which was rescued in *agl24-1 emf2-10 vrn2-1* triple mutants. These findings are consistent with the hypothesis that PcG proteins silence

478 *AGL24* but also other floral repressor genes to prevent the downregulation of several flower
479 development genes (**Fig. 7**).

480

481 **Ectopic *AGL24* expression results in *ap1*-like floral reversion in *emf2-10 vrn2-1* mutants and**
482 **might contribute to other reversion phenotypes in plants with strongly depleted PcG activity**

483 Overexpression of *AGL24* causes an *ap1*-like floral reversion phenotype with ectopic flowers in the
484 axil of first whorl organs and FM indeterminacy that is not a characteristic of *ap1* mutants (Yu et al.,
485 2004; Irish and Sussex, 1990; Liu et al., 2007). Therefore, we concluded that high expression of *AGL24*
486 causes at least partially the *ap1*-like floral reversion and FM indeterminacy in flowers with strongly
487 depleted PcG activity, which we confirmed by genetic and expression analysis. In PcG double mutants,
488 the partial loss of flowering commitment results in different types of floral reversion including ectopic
489 inflorescences inside of siliques (Müller-Xing et al., 2014; Müller-Xing et al., 2015). Remarkably,
490 overexpression of *AGL24* can result in similar FM-to-IM reversion independently of the daylength
491 condition (Yu et al., 2004). With the exception of the *ap1*-like phenotype, *emf2-10 vrn2-1* mutants
492 display floral reversions only under noninductive short day conditions (Müller-Xing et al., 2014;
493 Müller-Xing et al., 2015). Thus, the ectopic expression of *AGL24* is not sufficient for FM-to-IM
494 reversion in *emf2-10 vrn2-1* mutants (at least in long day). Previously, we showed that the activities of
495 two other MADS TF genes, *FLC* and *SVP*, are critical for the floral reversion in *emf2-10 vrn2-1* mutants
496 under noninductive conditions, whereas ectopic *FLC* represses *FT* that is required for maintaining the
497 commitment to flowering (Liu et al., 2014a; Müller-Xing et al., 2014). Notably, the previous genetic
498 analysis revealed that at least one other PcG target is involved (Müller-Xing et al., 2014), and *AGL24*
499 is a good candidate to act in parallel with *FLC* and *SVP* to promote daylength-dependent floral
500 reversion in PcG double mutants.

501

502 **PcG proteins promote FM determinacy by silencing of several floral regulators including *AGL24***
503 **and the pluripotency genes *WUS* and *STM***

504 Flower development requires initiation, maintenance and determinacy of the FM. The *CLV3*-*WUS*
505 feedback loop appears to be an intertwined and inseparable machinery that control the size of the
506 organizing center (marked by *WUS* expression) and stem cell domain (marked by *CLV3* expression),
507 which maintains all shoot meristems (Brand et al., 2000; Schoof et al., 2000). Most studies of FM

508 determinacy focused on the directly or indirectly transcriptional and epigenetic silencing of *WUS* in
509 floral stage 6 (Lenhard et al., 2001; Lohmann et al., 2001; Zhao et al., 2007; Sun et al., 2009; Ji et al.,
510 2011; Liu et al., 2011; Yumul et al., 2013; Liu et al., 2014b; Sun et al., 2014; Huang et al., 2017;
511 Yamaguchi et al., 2018; Fal et al., 2019; Sun et al., 2019). Nonetheless, we found that in the enlarged
512 IM and FMs of PcG double mutants the expression domain of *CLV3* was expanded, while *WUS*
513 expression and domain size were decreased indicating uncoupling of stem cell fate and *WUS* expression
514 levels. Our ChIP-Seq data revealed a large number of TFs that gaining H3K27me3 during FM
515 determinacy indicating that PcG proteins have a broader function than just silencing of *WUS*. Within
516 the TF genes with increased H3K27me3 levels, we found several HD and MADS genes known to
517 regulate FM determinacy including the floral repressor *AGL24* and the pluripotency genes *WUS* and
518 *STM* (Clark et al., 1993; Mayer et al., 1998; Laux et al., 1996; Yu et al., 2004). Although it was
519 suggested that PRC1 directly represses *STM* (Xu and Shen, 2008), *STM* is neither a H2Aub target gene
520 nor does the loss of PRC1 activity result in depletion of H3K27me3 at the *STM* locus (Xu and Shen,
521 2008; Bratzel et al., 2010; Zhou et al., 2017). In contrast, we showed that the *STM* locus accumulated
522 during early flower development high H3K27me3 levels that were reduced in *emf2-10 vrn2-1* double
523 mutants, while *STM* expression in FMs was temporally extended and maintained beyond flower stage
524 6. This suggests that PRC2-mediated H3K27me3 accumulation is the key silencing mechanism for
525 *STM* during FM determinacy.

526 Since loss of either *WUS* or *STM* is sufficient for premature FM arrest, it appears redundant to
527 silence both and other TF genes that are implied to promote meristem activity such as *AGL24*.
528 Nevertheless, our genetic analysis demonstrates that PcG proteins acts through *AGL24*, *STM*, and *WUS*
529 in floral determinacy. Some hypotheses about the necessity to silence so many TF genes can be drawn
530 from the features of the floral gene regulatory network: (I) Proper flower development also requires
531 silencing of genes well before FM determinacy during flower stage 6, such as *TFL1* at the onset of
532 flower morphogenesis, and *AGL24* after floral stage 2, since the repression of *AGL24* is essential for
533 the activation of the BCE-type MADS box genes to avoid homeotic transformations. (II) On the other
534 hand, due to the many positive and negative feedback loops in the gene regulatory network,
535 simultaneous silencing of pluripotency genes might be required to avoid compensatory loops such as
536 we described for *WUS* (Müller et al., 2006). The uncoupling of stem cell fate and *WUS* expression
537 levels, which we described here for *emf2-10 vrn2-1* mutant flowers, might be a result of a different
538 compensatory loop. (III) Both, *wus* and *stm* single mutants display limited organogenesis such as their
539 seedlings produce one to three leaves before meristem arrest and flowers bear a number of floral organs.

This indicates a certain delay in stem cell termination. Furthermore, *WUS* and *STM*, but also other pluripotency genes such as *PNY* and *PNF*, maintain FMs and the floral stem cell pool through distinct mechanisms (Endrizzi et al., 1996; Ung et al., 2011). Therefore, we propose that synchronized silencing of several pluripotency genes can accelerate FM determinacy in a way that cannot be achieved by silencing *WUS* alone.

545

Table 1 | Selection of TF genes, encoding known or putative floral meristem regulators, which gained H3K27me3 and were significantly reduced in expression during FM arrest

Gene Annotation		H3K27me3 (RPKM)		
Gene ID	**Name**	**t0**	**t5**	**FC**
A) HD TF genes				
AT5G02030	*PENNYWISE* (*PNY / BLR / RPL*)	**6.3 ± 0.4**	**46.9 ± 2.2**	**7.4**
AT1G23380	*KNOTTED-like from Arabidopsis thaliana 6* (*KNAT6*)	**5.7 ± 0.1**	**35.4 ± 4.3**	**6.2**
AT1G70510	*KNOTTED-like from Arabidopsis thaliana 2* (*KNAT2*)	**5.4 ± 0.2**	**24.6 ± 2.5**	**4.5**
AT1G62360	*SHOOT MERISTEMLESS* (*STM*)	**46.9 ± 1.3**	**116.0 ± 2.0**	**2.5**
AT2G27990	*POUND-FOOLISH* (*PNF / BLH8*)	**8.7 ± 0.3**	**21.3 ± 0.6**	**2.4**
AT4G08150	*BREVIPEDICELLUS* (*BP / KNAT1*)	**26.1 ± 1.3**	**52.7 ± 3.6**	**2.0**
AT5G41410	*BELL 1* (*BEL1*)	**50.1 ± 0.1**	**78.9 ± 0.7**	**1.6**
AT2G33880	*STIMPY* (*STIP / WOX9*)	**94.2 ± 2.4**	**136.3 ± 2.7**	**1.4**
B) MADS TF genes				
AT5G62165	*FOREVER YOUNG FLOWER* (*FYF / AGL42*)	**10.5 ± 0.3**	**47.3 ± 6.3**	**4.5**
AT5G60910	*FRUITFULL* (*FUL / AGL8*)	**8.8 ± 0.7**	**36.8 ± 4.0**	**4.2**
AT2G45660	*SUPPRESSOR OF OVEREXPRESSION OF CONSTANS 1* (*SOC1 / AGL20*)	**4.7 ± 0.2**	**18.9 ± 3.7**	**4.0**
AT2G22540	*SHORT VEGETATIVE PHASE* (*SVP*)	**40.0 ± 2.1**	**110.2 ± 14.4**	**2.8**
AT4G24540	*AGAMOUS-LIKE 24* (*AGL24*)	**40.7 ± 3.5**	**93.7 ± 7.3**	**2.3**
AT1G26310	*CAULIFLOWER* (*CAL / AGL10*)	**44.2 ± 0.1**	**73.7 ± 10.6**	**1.7**
AT5G51860	*AGAMOUS-LIKE 72* (*AGL72*)	**62.7 ± 0.2**	**84.1 ± 8.7**	**1.3**
C) Other TFs				
AT2G31160	*ORGAN BOUNDARY 1* (*OBO1 / LSH3*)	**6.6 ± 0.2**	**111.5 ± 11.1**	**16.8**
AT5G28490	*ORGAN BOUNDARY 2* (*OBO2 / LSH1*)	**38.8 ± 0.5**	**190.3 ± 18.9**	**4.9**
AT5G03840	*TERMINAL FLOWER1* (*TFL1*)	**49.0 ± 0.4**	**118.7 ± 11.2**	**2.4**
AT4G35900	*FD* (*ATBZIP14*)	**4.5 ± 0.5**	**9.7 ± 0.2**	**2.2**

546

547 Selection of TF genes that were gaining H3K27me3 (ChIP Seq) and significantly reduced in expression (Ryan et al., 2015)
548 during early flower development. The complete data for 151 genes are listed in Supplementary Table S5. FC, fold change
549 (t5/t0: floral stage 7-IM).

550

Figures

Fig. 1. Pleiotropic defects in flowers with strongly depleted PcG activity.

Fig. 2. Effects by strong PcG deficiency on meristem size and FM indeterminacy and genetic interaction with loss of *CLV3* function.

Fig. 3. Genome-wide changes of H3K27me3 levels during early flower development.

Fig. 4. Correlation of genome-wide changes in H3K27me3 levels and gene expression during early flower morphogenesis.

Fig. 5. Misexpression of *AGL24* represses several PcG target genes partially causing FM reversion and indeterminacy in PcG mutants.

Fig. 6. *STM* contributes to FM indeterminacy in PcG mutants.

Fig. 7. Concept of epigenetic (co)regulation of the floral gene regulatory network of TFs by PRC2 (H3K27me3).

Supplementary data

The following supplementary data are available at **JXB online**.

Supplementary Figure S1 | Test of the internal control *eIF4A* by *TIP41*, *RTFbox* and *UBQ10* (RT-qPCR).

Supplementary Figure S2 | Pleiotropic phenotype of *iCLF* flowers.

Supplementary Figure S3 | Increased size of vegetative SAM, IM and FMs in *emf2-10 vrn2-1* (*ev*) mutants.

Supplementary Figure S4 | Enhancement of the valveless phenotype in *emf2-10 vrn2-1 clv3-2* triple mutants.

Supplementary Figure S5 | *clv*/*crn emf2-10 vrn2-1* (*ev*) triple mutant flowers.

Supplementary Figure S6 | Validation of *35S::AP1-GR ap1-1 cal-1* samples before H3K27me3 ChIP Seq comparing undifferentiated IM tissue (t0) and differentiated flower tissue, five days after induction (t5, floral stage 7).

Supplementary Figure S7 | ChIP Seq Cluster analysis (DiffBind).

Supplementary Figure S8 | Changes of expression and H3K27me3 levels at MADS box and Homeobox genes during early flower development - ChIP Seq and qPCR validation data.

Supplementary Figure S9 | H3K27me3 levels of the *AG-WUS* feedback loop.

Supplementary Figure S10 | Venn diagram comparing H3K27me3 ChIP-seq data (t5) and gene expression (t5) (Ryan et al., 2015).

Supplementary Figure S11 | Venn diagram comparing published target genes of key floral TFs and H3K27me3 targets.

Supplementary Figure S12 | ChIP-qPCR of H3K27me3 level at TF genes in *emf2-10 vrn2-1* (*ev*).

Supplementary Figure S13 | Expression the 12 HD and nine MADS TF genes, which gained H3K27me3 and decreased in expression during early flower development, in *emf2-10 vrn2-1* (*ev*) inflorescence tips using RT-qPCR.

Supplementary Figure S14 | *LFY* misexpression in *emf2-10 vrn2-1* (*ev*).

590 **Supplementary Figure S15 | Genetic interaction of strong PcG deficiency and loss of A-function**
591 **during flower development.**

592 **Supplementary Figure S16 | Loss of H3K27me3 at *AGL24* locus in *emf2-10 vrn2-1* (*ev*)**
593 **inflorescences.**

594 **Supplementary Figure S17 | Expression of *AGL24* and *STM* in *clf-28 swn-7* callus-like tissue and**
595 ***iCLF* inflorescences.**

596 **Supplementary Figure S18 | Rescue of the extra floral organ phenotype in *iCLF* by loss of *STM***
597 **(*bum1-3* mutants).**

598

599 **Supplementary Table S1 | Primer list for RT-qPCR**

600 **Supplementary Table S2 | Primer list for ChIP-qPCR**

601 **Supplementary Table S3 | Differentially methylated regions (broad peaks) identified by**
602 **DiffBind with the DESeq2 method (p-value < 0.05)**

603 **Supplementary Table S4 | Differentially methylated genes (DMG) identified by**
604 **ChIPseekerSupplementary Table S5 | List of coding genes with increasing H3K27me3 and**
605 **decreasing expression levels during early flower development**

606 **Supplementary Table S6 | List of coding genes with decreasing H3K27me3 and increasing**
607 **expression levels during early flower development**

608 **Supplementary Table S7 | miRNA genes changing H3K27me3 levels during early flower**
609 **development**

610 **Supplementary Table S8 | Genes that are H3K27me3 targets in IM (t0) and/or flowers (t5, floral**
611 **stage 7)**

612 **Supplementary Table S9 | Carpel number and 5th whorl per silique in PcG and *STM* deficient**
613 **flowers (percent)**

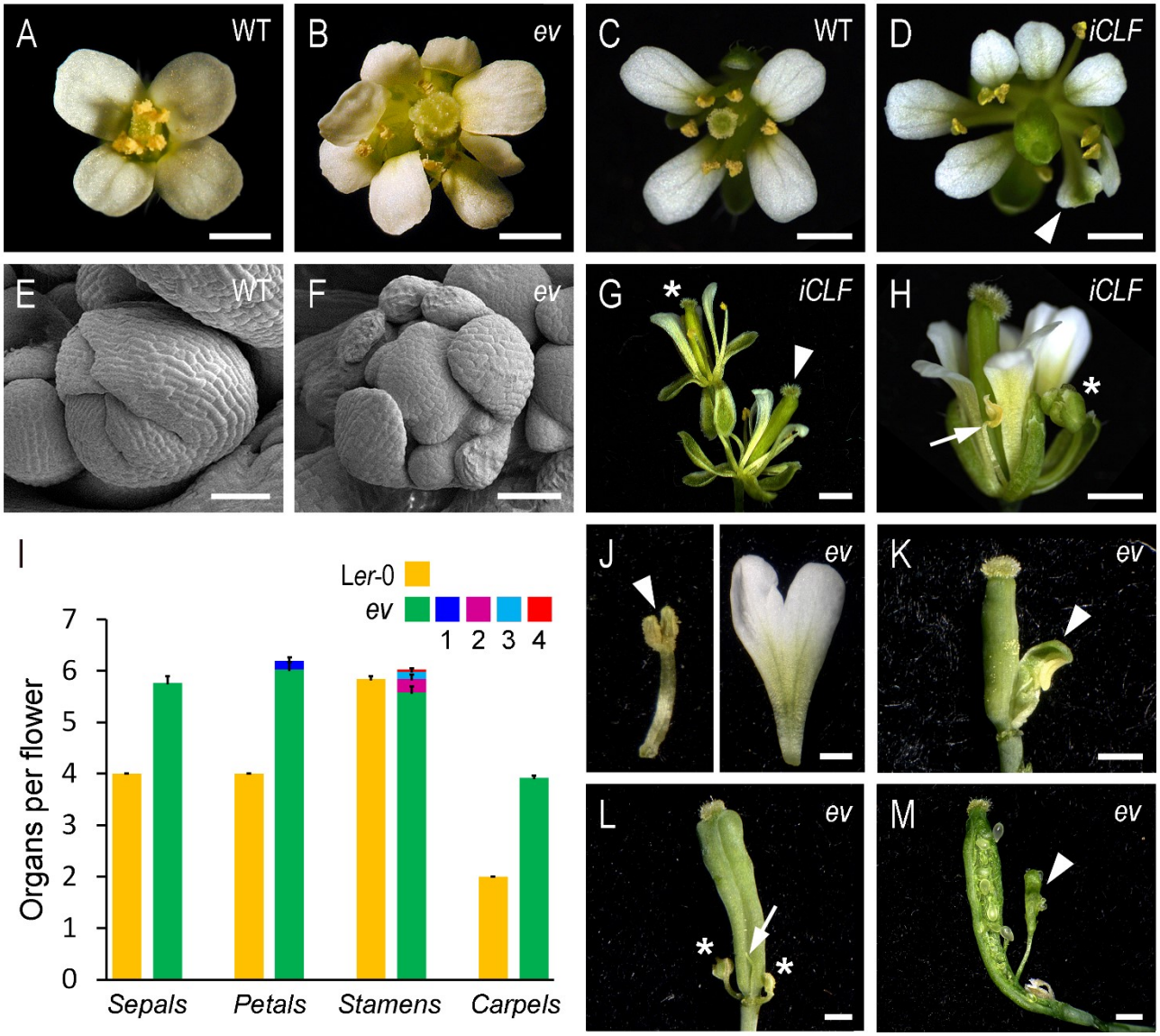

Fig. 1. Pleiotropic defects in flowers with strongly depleted PcG activity. (A-D) *emf2-10 vrn2-1* double mutant (*ev*) and *clf-28 swn-7 CLF-GR* (*iCLF*) flowers carrying extra floral organs including the well-visible petals in comparison to wild-type [WT: L*er*-0 **(A)** and Col-0 **(C)**] flowers with four white petals. **(D)** Arrowhead indicates a sepaloid petal. **(E-F)** Scanning electron micrographs of Ws-0 (WT) and *ev* flowers stage 11-12 (Smyth et al., 1990). Note that the sepals of *ev* are not closed. **(G-H)** *iCLF* flowers with petaloid stamen (arrow) and secondary flowers (asterisks) similar to *ap1* mutants; the arrowhead marks the primary flower. **(I)** Organ number in *ev* mutant flowers (green bars) compared with L*er*-0 flowers (orange bars) ± standard error of the mean (N = 50). 1, dark blue: sepaloid petals; 2, purple: flower organs with mixed staminoid and sepaloid identity; 3, light blue: filament without anthers; 4, red: stamen-carpel fusion. **(J)** Left panel: Two fused stamens (arrowhead). Right panel: Two fused petals. **(K)** Third whorl carpel fused with an anthers (arrowhead). **(L)** Silique with extra carpels after abscission of outer organs: Two secondary flowers (asterisks) and one filament (arrow) are marked. **(M)** *ev* silique, organs of a fifth whorl are visible (arrowhead) after cutting the silique open. Note that the flowers in **(A-B,I-M)** are *er* mutant. All scale bars = 1 mm with the exception of **(E-F)** = 100 µm.

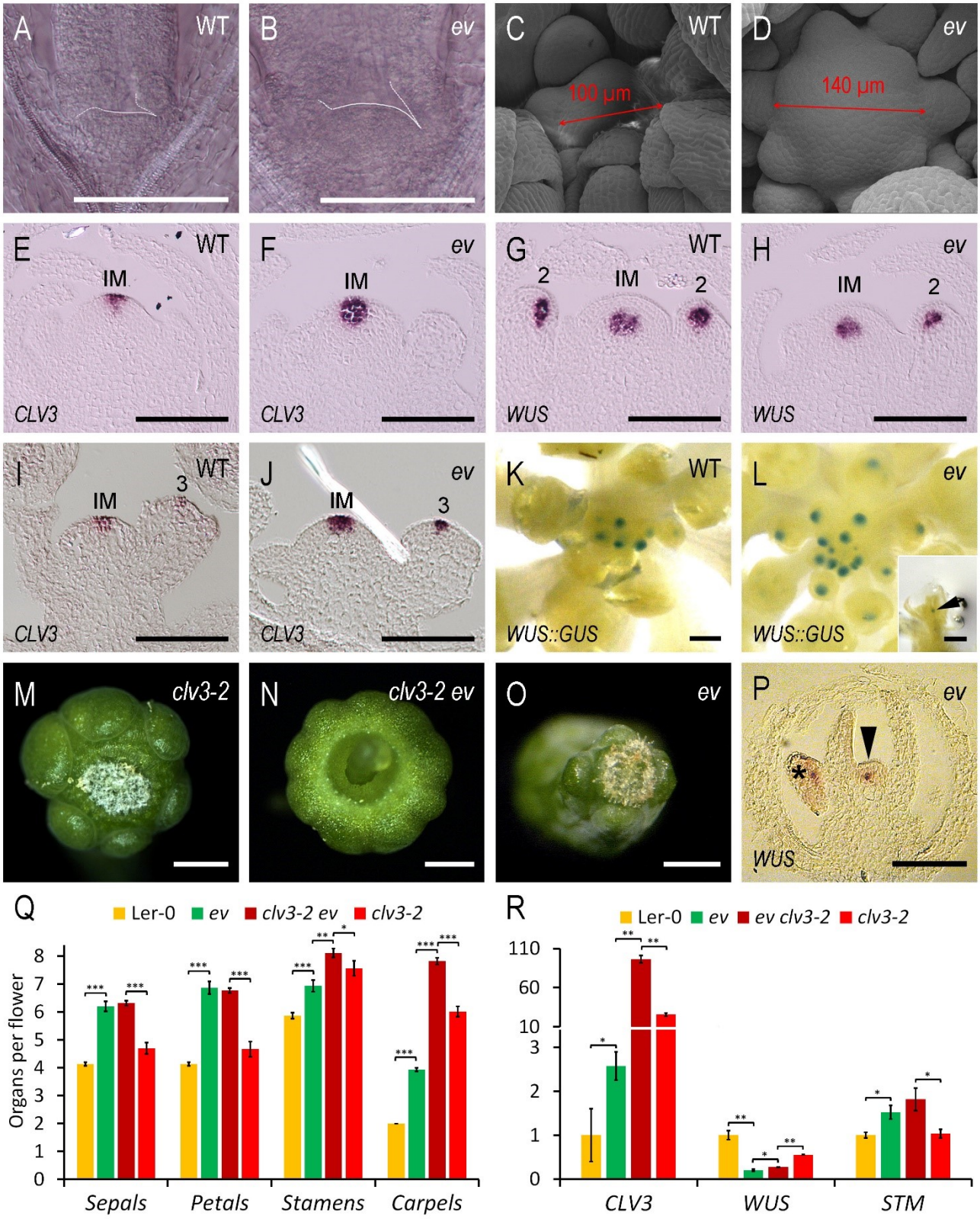

Fig. 2. Effects of strong PcG deficiency on meristem size and FM indeterminacy and genetic interaction with loss of *CLV3* function. (A-D) Increased meristem size of vegetative SAM **(A,B)** and IM **(C,D)** in *emf2-10 vrn2-1* (*ev*) mutants in comparison to wild-type (WT: Ws-0). **(E-J)** *CLV3* and *WUS* RNA *in situ* hybridizations in *ev* mutant IM and FMs in comparison to wild-type [WT: Ws-0 **(E,G)** and La-0 **(I)**]. **(K,L)** *WUS::GUS* staining in L*er*-0 and *emf2-10 vrn2-1* (*ev*). **(L)** In the inset, the

arrow indicates *WUS::GUS* expression in an *ev* flower with slotted gynoecial tube (floral stage ≥ 7 (Smyth et al., 1990)). **(M-O)** Additive increase of ectopic carpels in *clv3-2 emf2-10 vrn2-1* (*clv3-2 ev*) triple mutants. **(N)** Note that tissue of the fifth whorl grew out the unfused carpels. **(P)** *WUS* RNA *in situ* hybridizations of *ev* flower, stage 9 (Smyth et al., 1990). *WUS* is expressed in the indeterminate FM (arrow) and anthers (asterisk). **(Q)** Flower organs in *clv3-2 ev* triple mutants; ± standard error of the mean; N ≥ 30. **(R)** RT-qPCR analyses of gene expression in *clv3-2 ev* triple mutant inflorescence apices; columns indicate expression changes normalized by *elF4*, relative to expression in L*er*-0; ± standard error of the mean (N = 3). All scale bars = 100 µm with the exception of **(M-O)** = 1 mm.

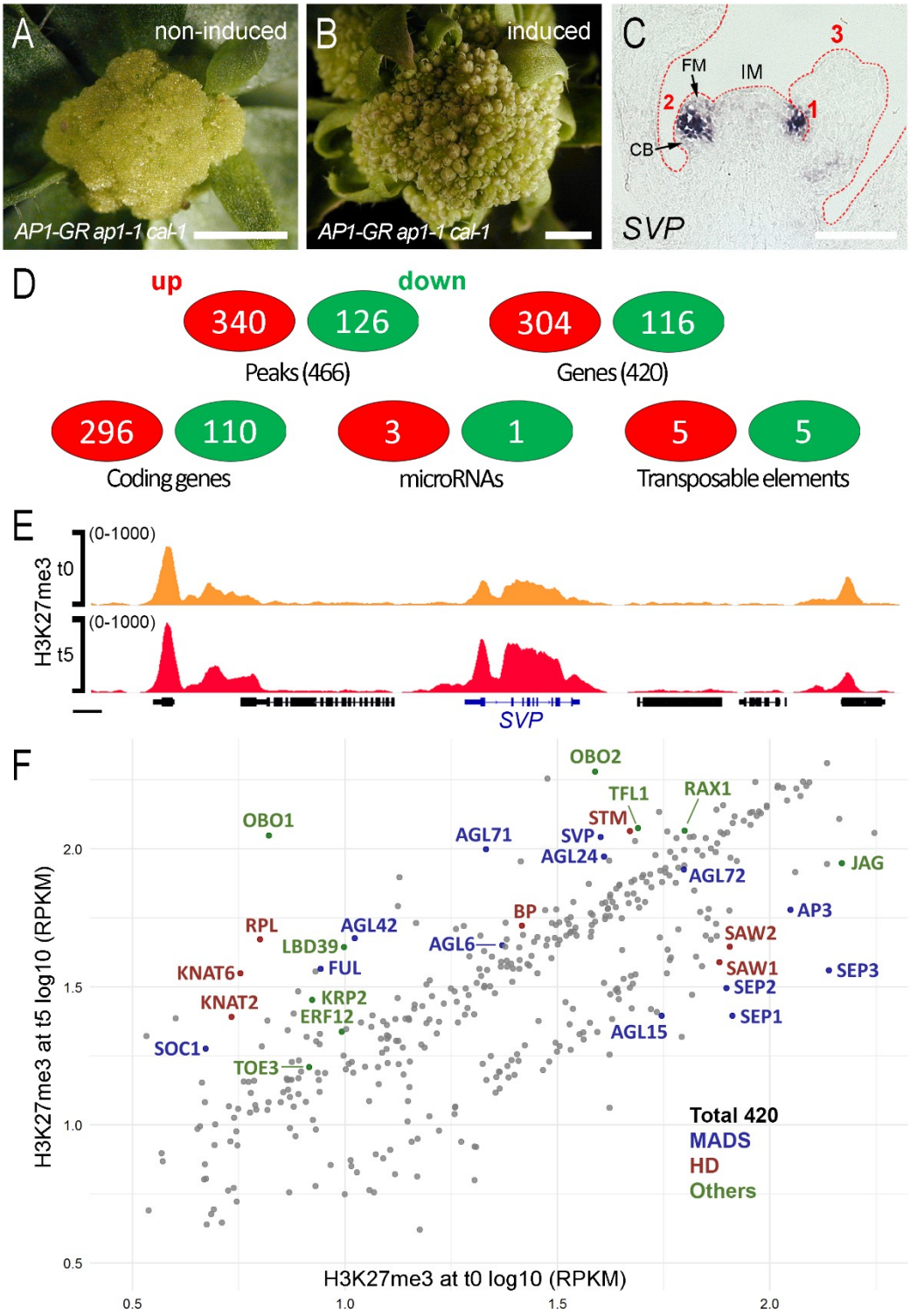

644 **Fig. 3. Genome-wide changes of H3K27me3 levels during early flower development. (A**,**B)** The
645 *AP1-GR ap1-1 cal-1* system (Wellmer et al., 2006) provide an enormous amount of either
646 undifferentiated inflorescence meristem **(A,** non-induced) and synchronized flower tissue **(B,** induced).
647 **(C)** *SVP* RNA *in situ* RNA hybridization in a wild-type inflorescence grown under LD conditions. *SVP*
648 is expressed throughout stage 1 floral primordia (1) whereas in stage 2 flower primordia (2), the *SVP*
649 expression domain divides flower meristem (FM) and cryptic bract (CB). Note that *SVP* is not
650 expressed in flower primordia stage 3 or older; IM, inflorescence meristem. **(D-F)** *AP1-GR ap1-1 cal-*

651 *1* ChIP Seq data. **(D)** Number of differentially methylated peaks (identified by DiffBind) and gene loci
652 (identified by ChIPseeker) encoding proteins, microRNAs or transposable elements. The differentially
653 methylated peaks and genes are listed in Supplementary Table S3 and S4, respectively. A cluster
654 analysis (DiffBind) can be found in Supplementary Fig. S7. **(E)** Close-up of the genomic region
655 containing the *SVP* locus (blue). H3K27me3 levels at *SVP* increased significantly, whereas neither of
656 the neighboring H3K27me3 target sites showed significant changes. **(F)** Comparison of all H3K27me3
657 target genes that are differentially methylated in IMs (t0) and flowers, stage 7 (t5). Each point
658 represents an H3K27me3 enriched gene. ChIP-Seq data were normalized to RPKM. Genes encoding
659 MADS domain TFs (blue), homeodomain (HD) TFs (red) or other proteins of interest (green) are
660 indicated.

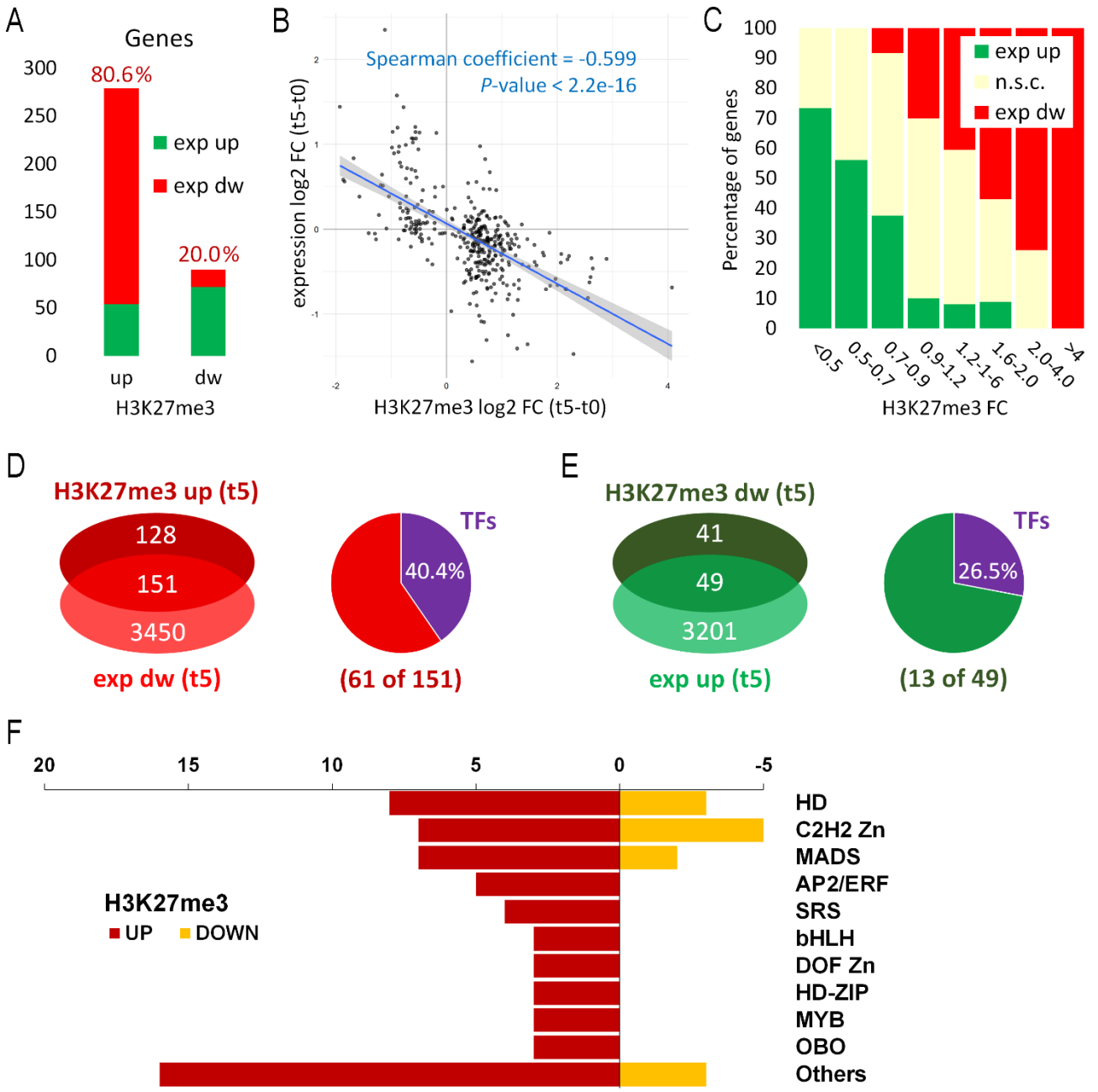

Fig. 4. Correlation of genome-wide changes in H3K27me3 levels and gene expression during early flower morphogenesis. (A-C) Correlation of DMGs and gene expression (Ryan et al., 2015). (**A**) Bar diagram of all DMG sorted by gain (up) and loss (dw) of H3K27me3. (**B**) Spearman correlation graph. (**C**) The DMGs are sorted by fold change of H3K27me3 levels. N: Numbers indicate the number of in each fold change (FC) category. **(D,E)** Venn diagrams (left) presenting the overlap of all coding genes with significant changes in H3K27me3 levels and gene expression (Ryan et al., 2015). Pie charts (right) presenting the overrepresentation of transcription factors (TFs) in the groups of overlap. **(F)** Distribution of TFs, which significantly changed H3K27me3 and anti-correlation in expression, sorted by TF gene families. FC, fold change. exp, expression. dw, down.

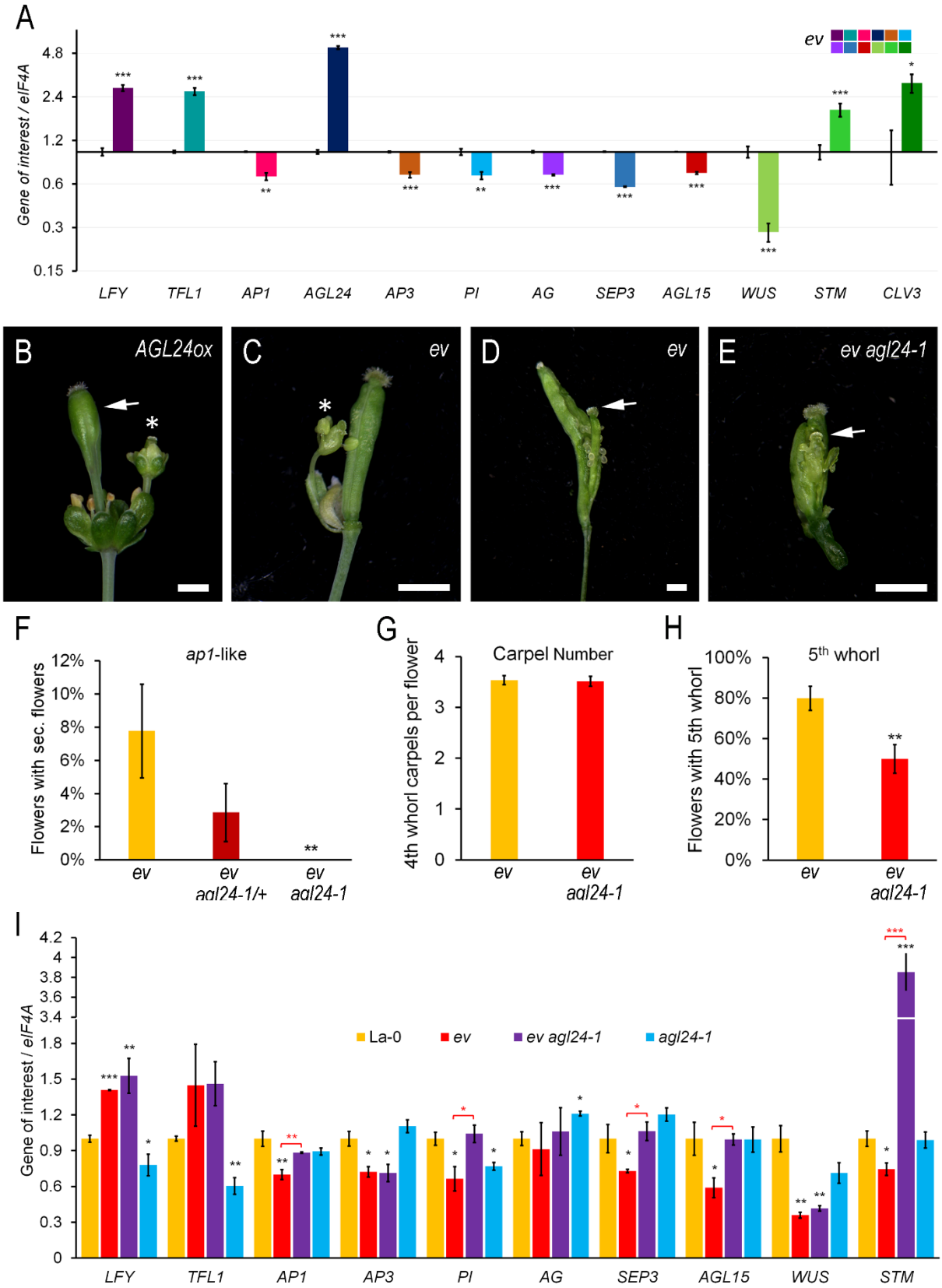

671 **Fig. 5. Misexpression of *AGL24* represses several PcG target genes partially causing FM**
672 **reversion and indeterminacy in PcG mutants. (A)** RT-qPCR analyses, gene expression of TFs and
673 *CLV3* in *emf2-10 vrn2-1* florescence apices; columns indicate expression changes in *emf2-10 vrn2-1*

normalized by *elF4A*, relative to expression in L*er*-0. Note the logarithmic scale. **(B)** Overexpression of *AGL24* results in indeterminate flowers carrying swollen siliques with a fifth whorl inside (arrow) and *ap1*-like secondary flowers (asterisk). **(C)** Most *ev* flowers carrying a fifth whorl and a few of them displays *ap1*-like flowers (asterisk). **(D-E)** *emf2-10 vrn2-1* (*ev*) and *emf2-10 vrn2-1 agl24-1* (*ev agl24-1*) siliques. The arrows mark the dissected fifth whorl carpels. **(F)** Percentage of the *ap1*-like flower phenotype in *ev*, *ev agl24-1/+* and *ev agl24-1* ($N \geq 70$). **(G)** Carpel number in *ev* and *ev agl24-1* ($N = 50$). **(H)** Percentage of flowers with fifth whorl in *ev* and *ev agl24-1* ($N = 50$). **(I)** RT-qPCR analyses of gene expression in *ev agl24-1* triple in comparison to *ev* double mutant inflorescence apices; columns indicate expression levels normalized by *elF4*, relative to expression in La-0. **(A,I)** All RT-qPCR experiments were performed with at least three biological replicates. **(A,F,H,I)** Asterisks indicate significant changes (Student's *t* test: *, $p \leq 0.05$; **, $p \leq 0.01$; ***, $p \leq 0.001$). All scale bars = 1 mm.

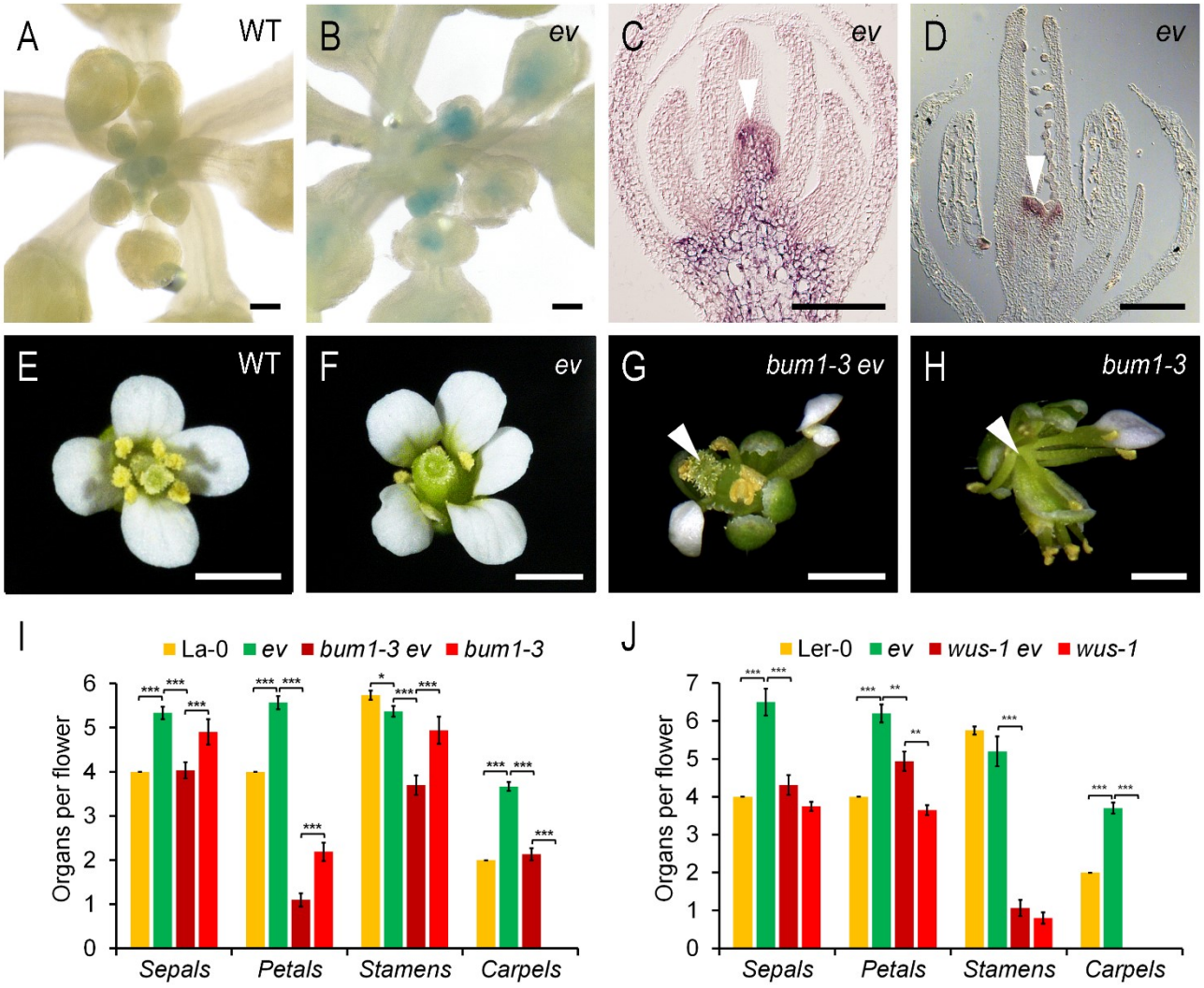

Fig. 6. *STM* contributes to FM indeterminacy in PcG mutants. (A,B) *STM::GUS* staining of WT (L*er*-0) and *emf2-10 vrn2-1* (scale bars = 0.1 mm). **(C,D)** RNA *in situ* hybridizations of *emf2-10 vrn2-1* flowers with *STM*. In contrast to wild-type, FMs of *emf2-10 vrn2-1* mutants remain indeterminate after stage six. *STM* expression (arrowheads) in indeterminate FM, floral stage 10 **(C)**, and floral stage 15 **(D)**. **(E-I)** Flower organs in *bum1-3 ev* triple mutants; ± standard error of the mean ($N \geq 30$). **(J)** Flower organs in *wus-1 ev* triple mutants; ± standard error of the mean ($N \geq 14$). Asterisks indicate

significant changes (Student's *t* test: *, $p \leq 0.05$; **, $p \leq 0.01$; ***, $p \leq 0.001$). Scale bars = 100 µm **(A-D)** and 1 mm **(E-H)**.

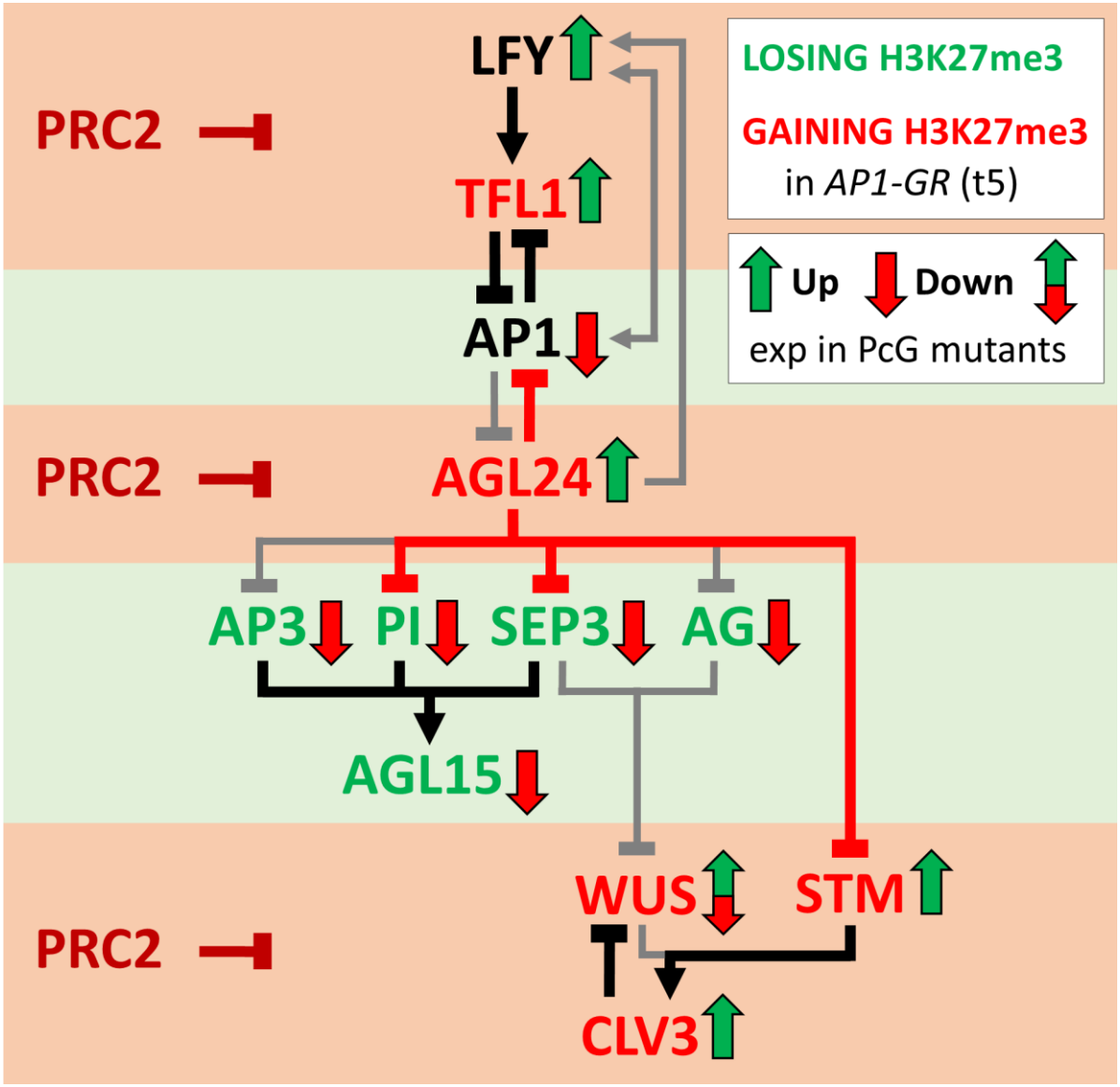

Fig. 7. Concept of epigenetic (co)regulation of the floral gene regulatory network of TFs by PRC2 (H3K27me3). Hierarchic model of the gene regulatory network with alternating regulation levels of gene silencing by PRC2 activity and gene activation during early flower development. Note that PRC2 activity can indirectly activate genes by silencing of transcriptional repressors like TFL1 and AGL24. Arrows, transcriptional activation. Arrows with blunt ends represent repression. Red arrows with blunt ends indicate repression by AGL24 in flowers with strongly depleted PcG activity. Grey arrows represent known transcriptional regulation in wild-type, which were suppressed in the strongly PcG-deficient background. Framed arrows: green, upregulated expression, and red, downregulated expression in *emf2-10 vrn2-1* double mutants (PcG). Note that although *WUS* expression is reduced in strongly PcG-deficient IMs and FMs, *WUS* is prolonged expressed in the indeterminate FMs.

Acknowledgments

Seeds were kindly provided by Frank Wellmer, Yuling Jiao and Wolfgang Werr. We thank Marc Somssich for critical reading and comments on the manuscript and Rüdiger Simon for sharing plasmids for RNA *in situ* hybridisation. The authors would like to thank the HPC Service of ZEDAT, Freie Universität Berlin, for computing time. This work was kindly funded by the National Natural Science Foundation of China (project nos 31640054 and 31771602), the Fundamental Research Funds for the Central Universities (project no. 2572020DY06) and the Northeast Forestry University Starting Grant for Distinguished Young Scholars.

Author Contributions

All authors performed the experiments. RMX and JG designed the experiments. RMX and QX wrote the manuscript with the help of RA and JT. LV and GW performed the bioinformatics analysis with the technical support of SC and SC.

Data availability

The ChIP-seq data was deposited in the Gene Expression Omnibus under the series GSE159988. All other relevant data are available within the paper and its supplementary data published online.

1 References

Alvarez-Buylla, E. R., Benítez, M., Corvera-Poiré, A., Chaos Cador, A., Folter, S. de, **Gamboa de Buen, A., Garay-Arroyo, A., García-Ponce, B., Jaimes-Miranda, F., Pérez-Ruiz, R. V. et al.** (2010). Flower development. *The arabidopsis book* **8**, e0127.

Baroux, C., Gagliardini, V., Page, D. R. and Grossniklaus, U. (2006). Dynamic regulatory interactions of Polycomb group genes. MEDEA autoregulation is required for imprinted gene expression in Arabidopsis. *Genes & development* **20**, 1081–1086.

Bennett, L., Melchers, B. and Proppe, B. (2020). Curta. A General-purpose High-Performance Computer at ZEDAT, Freie Universität Berlin.

Blázquez, M. A., Soowal, L. N., Lee, I. and Weigel, D. (1997). LEAFY expression and flower initiation in Arabidopsis. *Development (Cambridge, England)* **124**, 3835–3844.

Bradley, D., Ratcliffe, O., Vincent, C., Carpenter, R. and Coen, E. (1997). Inflorescence commitment and architecture in Arabidopsis. *Science (New York, N.Y.)* **275**, 80–83.

Brand, U., Fletcher, J. C., Hobe, M., Meyerowitz, E. M. and Simon, R. (2000). Dependence of stem cell fate in Arabidopsis on a feedback loop regulated by CLV3 activity. *Science (New York, N.Y.)* **289**, 617–619.

Bratzel, F., López-Torrejón, G., Koch, M., Del Pozo, J. C. and Calonje, M. (2010). Keeping cell identity in Arabidopsis requires PRC1 RING-finger homologs that catalyze H2A monoubiquitination. *Current biology : CB* **20**, 1853–1859.

Causier, B., Schwarz-Sommer, Z. and Davies, B. (2010). Floral organ identity. 20 years of ABCs. *Seminars in cell & developmental biology* **21**, 73–79.

Chanvivattana, Y., Bishopp, A., Schubert, D., Stock, C., Moon, Y.-H., Sung, Z. R. and Goodrich, J. (2004). Interaction of Polycomb-group proteins controlling flowering in Arabidopsis. *Development (Cambridge, England)* **131**, 5263–5276.

Chu, T., Xie, H., Xu, Y. and Ma, R. (2010). Regulation pattern of the FRUITFULL (FUL) gene of Arabidopsis thaliana. *Chinese journal of biotechnology* **26**, 1546–1554.

Clark, S. E., Running, M. P. and Meyerowitz, E. M. (1993). CLAVATA1, a regulator of meristem and flower development in Arabidopsis. *Development (Cambridge, England)* **119**, 397–418.

Clark, S. E., Running, M. P. and Meyerowitz, E. M. (1995). CLAVATA3 is a specific regulator of shoot and floral meristem development affecting the same processes as CLAVATA1. *Development (Cambridge, England)* **121**, 2057–2067.

Coen, E. S. and Meyerowitz, E. M. (1991). The war of the whorls. Genetic interactions controlling flower development. *Nature* **353**, 31–37.

Daum, G., Medzihradszky, A., Suzaki, T. and Lohmann, J. U. (2014). A mechanistic framework for noncell autonomous stem cell induction in Arabidopsis. *Proceedings of the National Academy of Sciences of the United States of America* **111**, 14619–14624.

Di Sun, Li, Y., Ma, Z., Yan, X., Li, N., Shang, B., Hu, X., Cui, K., Koiwa, H. and Zhang, X. (2021). The epigenetic factor FVE orchestrates cytoplasmic SGS3-DRB4-DCL4 activities to promote transgene silencing in Arabidopsis. *Sci. Adv.* https://doi.org/10.1126/sciadv.abf3898.

Diévart, A., Dalal, M., Tax, F. E., Lacey, A. D., Huttly, A., Li, J. and Clark, S. E. (2003). CLAVATA1 dominant-negative alleles reveal functional overlap between multiple receptor kinases that regulate meristem and organ development. *The Plant cell* **15**, 1198–1211.

Ditta, G., Pinyopich, A., Robles, P., Pelaz, S. and Yanofsky, M. F. (2004). The SEP4 gene of Arabidopsis thaliana functions in floral organ and meristem identity. *Current biology : CB* **14**, 1935–1940.

Endrizzi, K., Moussian, B., Haecker, A., Levin, J. Z. and Laux, T. (1996). The SHOOT MERISTEMLESS gene is required for maintenance of undifferentiated cells in Arabidopsis shoot and floral meristems and acts at a different regulatory level than the meristem genes WUSCHEL and ZWILLE. *Plant J* **10**, 967–979.

Engelhorn, J., Blanvillain, R., Kröner, C., Parrinello, H., Rohmer, M., Posé, D., Ott, F., Schmid, M. and Carles, C. (2017). Dynamics of H3K4me3 Chromatin Marks Prevails over H3K27me3 for Gene Regulation during Flower Morphogenesis in Arabidopsis thaliana. *Epigenomes* **1**, 8.

Fal, K., Cortes, M., Liu, M., Collaudin, S., Das, P., Hamant, O. and Trehin, C. (2019). Paf1c defects challenge the robustness of flower meristem termination in Arabidopsis thaliana. *Development (Cambridge, England)*. https://doi.org/10.1242/dev.173377.

Fletcher, J. C., Brand, U., Running, M. P., Simon, R. and Meyerowitz, E. M. (1999). Signaling of cell fate decisions by CLAVATA3 in Arabidopsis shoot meristems. *Science (New York, N.Y.)* **283**, 1911–1914.

Gaspar, J. M. (2018). Improved peak-calling with MACS2. *bioRxiv*. https://doi.org/10.1101/496521.

Goslin, K., Zheng, B., Serrano-Mislata, A., Rae, L., Ryan, P. T., Kwaśniewska, K., Thomson, B., Ó'Maoiléidigh, D. S., Madueño, F., Wellmer, F. et al. (2017). Transcription Factor Interplay between LEAFY and APETALA1/CAULIFLOWER during Floral Initiation. *Plant physiology* **174**, 1097–1109.

Grandi, V., Gregis, V. and Kater, M. M. (2012). Uncovering genetic and molecular interactions among floral meristem identity genes in Arabidopsis thaliana. *The Plant journal : for cell and molecular biology* **69**, 881–893.

Gregis, V., Sessa, A., Colombo, L. and Kater, M. M. (2006). AGL24, SHORT VEGETATIVE PHASE, and APETALA1 redundantly control AGAMOUS during early stages of flower development in Arabidopsis. *The Plant cell* **18**, 1373–1382.

Gregis, V., Sessa, A., Colombo, L. and Kater, M. M. (2008). AGAMOUS-LIKE24 and SHORT VEGETATIVE PHASE determine floral meristem identity in Arabidopsis. *The Plant journal : for cell and molecular biology* **56**, 891–902.

Gregis, V., Sessa, A., Dorca-Fornell, C. and Kater, M. M. (2009). The Arabidopsis floral meristem identity genes AP1, AGL24 and SVP directly repress class B and C floral homeotic genes. *The Plant journal : for cell and molecular biology* **60**, 626–637.

Gross-Hardt, R., Lenhard, M. and Laux, T. (2002). WUSCHEL signaling functions in interregional communication during Arabidopsis ovule development. *Genes & development* **16**, 1129–1138.

Hartmann, U., Höhmann, S., Nettesheim, K., Wisman, E., Saedler, H. and Huijser, P. (2000). Molecular cloning of SVP. A negative regulator of the floral transition in Arabidopsis. *The Plant journal : for cell and molecular biology* **21**, 351–360.

Huang, Z., Shi, T., Zheng, B., Yumul, R. E., Liu, X., You, C., Gao, Z., Xiao, L. and Chen, X. (2017). APETALA2 antagonizes the transcriptional activity of AGAMOUS in regulating floral stem cells in Arabidopsis thaliana. *The New phytologist* **215**, 1197–1209.

Hugouvieux, V., Silva, C. S., Jourdain, A., Stigliani, A., Charras, Q., Conn, V., Conn, S. J., Carles, C. C., Parcy, F. and Zubieta, C. (2018). Tetramerization of MADS family transcription factors SEPALLATA3 and AGAMOUS is required for floral meristem determinacy in Arabidopsis. *Nucleic acids research* **46**, 4966–4977.

Immink, R. G. H., Tonaco, I. A. N., Folter, S. de, **Shchennikova, A., van Dijk, A. D. J., Busscher-Lange, J., Borst, J. W. and Angenent, G. C.** (2009). SEPALLATA3. The 'glue' for MADS box transcription factor complex formation. *Genome biology* **10**, R24.

Irish, V. F. and Sussex, I. M. (1990). Function of the apetala-1 gene during Arabidopsis floral development. *The Plant cell* **2**, 741–753.

Ji, L., Liu, X., Yan, J., Wang, W., Yumul, R. E., Kim, Y. J., Dinh, T. T., Liu, J., Cui, X., Zheng, B. et al. (2011). ARGONAUTE10 and ARGONAUTE1 regulate the termination of floral stem cells through two microRNAs in Arabidopsis. *PLoS genetics* **7**, e1001358.

Jing, T., Ardiansyah, R., Xu, Q., Xing, Q. and Müller-Xing, R. (2020). Reprogramming of Cell Fate During Root Regeneration by Transcriptional and Epigenetic Networks. *Front. Plant Sci.* **11**, 613.

Kaufmann, K., Wellmer, F., Muiño, J. M., Ferrier, T., Wuest, S. E., Kumar, V., Serrano-Mislata, A., Madueño, F., Krajewski, P., Meyerowitz, E. M. et al. (2010). Orchestration of floral initiation by APETALA1. *Science (New York, N.Y.)* **328**, 85–89.

Kayes, J. M. and Clark, S. E. (1998). CLAVATA2, a regulator of meristem and organ development in Arabidopsis. *Development (Cambridge, England)* **125**, 3843–3851.

Kempin, S. A., Savidge, B. and Yanofsky, M. F. (1995). Molecular basis of the cauliflower phenotype in Arabidopsis. *Science (New York, N.Y.)* **267**, 522–525.

Kirch, T., Simon, R., Grünewald, M. and Werr, W. (2003). The DORNRÖSCHEN/ENHANCER OF SHOOT REGENERATION1 Gene of Arabidopsis Acts in the Control of Meristem Cell Fate and Lateral Organ Development. *Plant Cell* **15**, 694–705.

Krizek, B. A., Bantle, A. T., Heflin, J. M., Han, H., Freese, N. H., Loraine, A. E. and Melzer, R. (2021). AINTEGUMENTA and AINTEGUMENTA-LIKE6 directly regulate floral homeotic, growth, and vascular development genes in young Arabidopsis flowers. *Journal of experimental botany* **72**, 5478–5493.

Lafos, M., Kroll, P., Hohenstatt, M. L., Thorpe, F. L., Clarenz, O. and Schubert, D. (2011). Dynamic regulation of H3K27 trimethylation during Arabidopsis differentiation. *PLoS genetics* **7**, e1002040.

Laux, T., Mayer, K. F., Berger, J. and Jürgens, G. (1996). The WUSCHEL gene is required for shoot and floral meristem integrity in Arabidopsis. *Development (Cambridge, England)* **122**, 87–96.

Lenhard, M., Bohnert, A., Jürgens, G. and Laux, T. (2001). Termination of stem cell maintenance in Arabidopsis floral meristems by interactions between WUSCHEL and AGAMOUS. *Cell* **105**, 805–814.

Liao, Y., Smyth, G. K. and Shi, W. (2014). featureCounts. An efficient general purpose program for assigning sequence reads to genomic features. *Bioinformatics* **30**, 923–930.

Liljegren, S. J., Gustafson-Brown, C., Pinyopich, A., Ditta, G. S. and Yanofsky, M. F. (1999). Interactions among APETALA1, LEAFY, and TERMINAL FLOWER1 specify meristem fate. *The Plant cell* **11**, 1007–1018.

Liu, C., Zhou, J., Bracha-Drori, K., Yalovsky, S., Ito, T. and Yu, H. (2007). Specification of Arabidopsis floral meristem identity by repression of flowering time genes. *Development (Cambridge, England)* **134**, 1901–1910.

Liu, C., Xi, W., Shen, L., Tan, C. and Yu, H. (2009). Regulation of floral patterning by flowering time genes. *Developmental cell* **16**, 711–722.

Liu, C., Teo, Z. W. N., Bi, Y., Song, S., Xi, W., Yang, X., Yin, Z. and Yu, H. (2013). A conserved genetic pathway determines inflorescence architecture in Arabidopsis and rice. *Developmental cell* **24**, 612–622.

Liu, L., Farrona, S., Klemme, S. and Turck, F. K. (2014a). Post-fertilization expression of FLOWERING LOCUS T suppresses reproductive reversion. *Frontiers in plant science* **5**, 164.

Liu, X., Kim, Y. J., Müller, R., Yumul, R. E., Liu, C., Pan, Y., Cao, X., Goodrich, J. and Chen, X. (2011). AGAMOUS terminates floral stem cell maintenance in Arabidopsis by directly repressing WUSCHEL through recruitment of Polycomb Group proteins. *The Plant cell* **23**, 3654–3670.

Liu, X., Dinh, T. T., Li, D., Shi, B., Li, Y., Cao, X., Guo, L., Pan, Y., Jiao, Y. and Chen, X. (2014b). AUXIN RESPONSE FACTOR 3 integrates the functions of AGAMOUS and APETALA2 in floral meristem determinacy. *The Plant journal : for cell and molecular biology* **80**, 629–641.

Li, X., Zheng, Y., Xing, Q., Ardiansyah, R., Zhou, H., Ali, S., Jing, T., Tian, J., Song, X. S., Li, Y. et al. (2020). Ectopic expression of the transcription factor CUC2 restricts growth by cell cycle inhibition in Arabidopsis leaves. *Plant signaling & behavior* **15**, 1706024.

Lohmann, J. U., Hong, R. L., Hobe, M., Busch, M. A., Parcy, F., Simon, R. and Weigel, D. (2001). A molecular link between stem cell regulation and floral patterning in Arabidopsis. *Cell* **105**, 793–803.

Lopez-Vernaza, M., Yang, S., Müller, R., Thorpe, F., Leau, E. de and **Goodrich, J.** (2012). Antagonistic roles of SEPALLATA3, FT and FLC genes as targets of the polycomb group gene CURLY LEAF. *PloS one* **7**, e30715.

Mayer, K. F., Schoof, H., Haecker, A., Lenhard, M., Jürgens, G. and Laux, T. (1998). Role of WUSCHEL in regulating stem cell fate in the Arabidopsis shoot meristem. *Cell* **95**, 805–815.

Melzer, R., Verelst, W. and Theissen, G. (2009). The class E floral homeotic protein SEPALLATA3 is sufficient to loop DNA in 'floral quartet'-like complexes in vitro. *Nucleic acids research* **37**, 144–157.

Michaels, S. D., Ditta, G., Gustafson-Brown, C., Pelaz, S., Yanofsky, M. and Amasino, R. M. (2003). AGL24 acts as a promoter of flowering in Arabidopsis and is positively regulated by vernalization. *The Plant journal : for cell and molecular biology* **33**, 867–874.

Ming, F. and Ma, H. (2009). A terminator of floral stem cells. *Genes & development* **23**, 1705–1708.

Moyroud, E., Minguet, E. G., Ott, F., Yant, L., Posé, D., Monniaux, M., Blanchet, S., Bastien, O., Thévenon, E., Weigel, D. et al. (2011). Prediction of regulatory interactions from genome

sequences using a biophysical model for the Arabidopsis LEAFY transcription factor. *The Plant cell* **23**, 1293–1306.

Mozgova, I. and Hennig, L. (2015). The polycomb group protein regulatory network. *Annual review of plant biology* **66**, 269–296.

Müller, R., Borghi, L., Kwiatkowska, D., Laufs, P. and Simon, R. (2006). Dynamic and compensatory responses of Arabidopsis shoot and floral meristems to CLV3 signaling. *The Plant cell* **18**, 1188–1198.

Müller, R., Bleckmann, A. and Simon, R. (2008). The receptor kinase CORYNE of Arabidopsis transmits the stem cell-limiting signal CLAVATA3 independently of CLAVATA1. *The Plant cell* **20**, 934–946.

Müller-Xing, R., Clarenz, O., Pokorny, L., Goodrich, J. and Schubert, D. (2014). Polycomb-Group Proteins and FLOWERING LOCUS T Maintain Commitment to Flowering in Arabidopsis thaliana. *The Plant cell* **26**, 2457–2471.

Müller-Xing, R., Schubert, D. and Goodrich, J. (2015). Non-inductive conditions expose the cryptic bract of flower phytomeres in Arabidopsis thaliana. *Plant signaling & behavior* **10**, e1010868.

Nägeli, C. (1858). Beiträge zur wissenschaftlichen Botanik. *Verlag von Wilhelm Engelmann* **1**, 2.

Pelaz, S., Ditta, G. S., Baumann, E., Wisman, E. and Yanofsky, M. F. (2000). B and C floral organ identity functions require SEPALLATA MADS-box genes. *Nature* **405**, 200–203.

Pelaz, S., Gustafson-Brown, C., Kohalmi, S. E., Crosby, W. L. and Yanofsky, M. F. (2001). APETALA1 and SEPALLATA3 interact to promote flower development. *The Plant journal : for cell and molecular biology* **26**, 385–394.

Ratcliffe, O. J., Bradley, D. J. and Coen, E. S. (1999). Separation of shoot and floral identity in Arabidopsis. *Development (Cambridge, England)* **126**, 1109–1120.

Ryan, P. T., Ó'Maoiléidigh, D. S., Drost, H.-G., Kwaśniewska, K., Gabel, A., Grosse, I., Graciet, E., Quint, M. and Wellmer, F. (2015). Patterns of gene expression during Arabidopsis flower development from the time of initiation to maturation. *BMC genomics* **16**, 488.

Schoof, H., Lenhard, M., Haecker, A., Mayer, K. F.X., Jürgens, G. and Laux, T. (2000). The Stem Cell Population of Arabidopsis Shoot Meristems Is Maintained by a Regulatory Loop between the CLAVATA and WUSCHEL Genes. *Cell* **100**, 635–644.

Schubert, D., Clarenz, O. and Goodrich, J. (2005). Epigenetic control of plant development by Polycomb-group proteins. *Current opinion in plant biology* **8**, 553–561.

Schuettengruber, B., Bourbon, H.-M., Di Croce, L. and Cavalli, G. (2017). Genome Regulation by Polycomb and Trithorax. 70 Years and Counting. *Cell* **171**, 34–57.

Scofield, S. and Murray, J. A. H. (2006). KNOX gene function in plant stem cell niches. *Plant molecular biology* **60**, 929–946.

Serrano-Mislata, A., Goslin, K., Zheng, B., Rae, L., Wellmer, F., Graciet, E. and Madueño, F. (2017). Regulatory interplay between LEAFY, APETALA1/CAULIFLOWER and TERMINAL FLOWER1. New insights into an old relationship. *Plant signaling & behavior* **12**, e1370164.

Shivram, H., Le, S. V. and Iyer, V. R. (2019). PRC2 activates interferon-stimulated genes indirectly by repressing miRNAs in glioblastoma. *PloS one* **14**, e0222435.

Smyth, D. R., Bowman, J. L. and Meyerowitz, E. M. (1990). Early flower development in Arabidopsis. *The Plant cell* **2**, 755–767.

Somssich, M., Je, B. I., Simon, R. and Jackson, D. (2016). CLAVATA-WUSCHEL signaling in the shoot meristem. *Development (Cambridge, England)* **143**, 3238–3248.

Soyars, C. L., James, S. R. and Nimchuk, Z. L. (2016). Ready, aim, shoot. Stem cell regulation of the shoot apical meristem. *Current opinion in plant biology* **29**, 163–168.

Spillane, C., MacDougall, C., Stock, C., Köhler, C., Vielle-Calzada, J. P., Nunes, S. M., Grossniklaus, U. and Goodrich, J. (2000). Interaction of the Arabidopsis polycomb group proteins FIE and MEA mediates their common phenotypes. *Current biology : CB* **10**, 1535–1538.

Stark, R. and Brown, G. (2011). DiffBind: differential binding analysis of ChIP-Seq peak data.

Sun, B., Xu, Y., Ng, K.-H. and Ito, T. (2009). A timing mechanism for stem cell maintenance and differentiation in the Arabidopsis floral meristem. *Genes & development* **23**, 1791–1804.

Sun, B., Looi, L.-S., Guo, S., He, Z., Gan, E.-S., Huang, J., Xu, Y., Wee, W.-Y. and Ito, T. (2014). Timing mechanism dependent on cell division is invoked by Polycomb eviction in plant stem cells. *Science (New York, N.Y.)* **343**, 1248559.

Sun, B., Zhou, Y., Cai, J., Shang, E., Yamaguchi, N., Xiao, J., Looi, L.-S., Wee, W.-Y., Gao, X., Wagner, D. et al. (2019). Integration of Transcriptional Repression and Polycomb-Mediated Silencing of WUSCHEL in Floral Meristems. *The Plant cell* **31**, 1488–1505.

Ung, N., Lal, S. and Smith, H. M. S. (2011). The role of PENNYWISE and POUND-FOOLISH in the maintenance of the shoot apical meristem in Arabidopsis. *Plant physiology* **156**, 605–614.

Velanis, C. N., Herzyk, P. and Jenkins, G. I. (2016). Regulation of transcription by the Arabidopsis UVR8 photoreceptor involves a specific histone modification. *Plant molecular biology* **92**, 425–443.

Wagner, D., Sablowski, R. W. and Meyerowitz, E. M. (1999). Transcriptional activation of APETALA1 by LEAFY. *Science (New York, N.Y.)* **285**, 582–584.

Wellmer, F., Alves-Ferreira, M., Dubois, A., Riechmann, J. L. and Meyerowitz, E. M. (2006). Genome-wide analysis of gene expression during early Arabidopsis flower development. *PLoS genetics* **2**, e117.

Williams, L. and Fletcher, J. C. (2005). Stem cell regulation in the Arabidopsis shoot apical meristem. *Current opinion in plant biology* **8**, 582–586.

Xiao, J., Jin, R. and Wagner, D. (2017). Developmental transitions. Integrating environmental cues with hormonal signaling in the chromatin landscape in plants. *Genome Biol* **18**, a019315.

Xu, L. and Shen, W.-H. (2008). Polycomb silencing of KNOX genes confines shoot stem cell niches in Arabidopsis. *Current biology : CB* **18**, 1966–1971.

Yadav, R. K., Perales, M., Gruel, J., Girke, T., Jönsson, H. and Reddy, G. V. (2011). WUSCHEL protein movement mediates stem cell homeostasis in the Arabidopsis shoot apex. *Genes & development* **25**, 2025–2030.

Yamaguchi, N., Huang, J., Tatsumi, Y., Abe, M., Sugano, S. S., Kojima, M., Takebayashi, Y., Kiba, T., Yokoyama, R., Nishitani, K. et al. (2018). Chromatin-mediated feed-forward auxin biosynthesis in floral meristem determinacy. *Nature communications* **9**, 5290.

Yan, Z., Shi, H., Liu, Y., Jing, M., Han, Y. and Wellmer, F. (2020). KHZ1 and KHZ2, novel members of the autonomous pathway, repress the splicing efficiency of FLC pre-mRNA in Arabidopsis. *Journal of experimental botany* **71**, 1375–1386.

Yu, G., Wang, L.-G. and He, Q.-Y. (2015). ChIPseeker. An R/Bioconductor package for ChIP peak annotation, comparison and visualization. *Bioinformatics* **31**, 2382–2383.

Yu, H., Ito, T., Wellmer, F. and Meyerowitz, E. M. (2004). Repression of AGAMOUS-LIKE 24 is a crucial step in promoting flower development. *Nature genetics* **36**, 157–161.

Yumul, R. E., Kim, Y. J., Liu, X., Wang, R., Ding, J., Xiao, L. and Chen, X. (2013). POWERDRESS and diversified expression of the MIR172 gene family bolster the floral stem cell network. *PLoS genetics* **9**, e1003218.

Zhang, X., Clarenz, O., Cokus, S., Bernatavichute, Y. V., Pellegrini, M., Goodrich, J. and Jacobsen, S. E. (2007). Whole-genome analysis of histone H3 lysine 27 trimethylation in Arabidopsis. *PLoS biology* **5**, e129.

Zhao, L., Kim, Y., Dinh, T. T. and Chen, X. (2007). miR172 regulates stem cell fate and defines the inner boundary of APETALA3 and PISTILLATA expression domain in Arabidopsis floral meristems. *The Plant journal : for cell and molecular biology* **51**, 840–849.

Zhou, Y., Romero-Campero, F. J., Gómez-Zambrano, Á., Turck, F. and Calonje, M. (2017). H2A monoubiquitination in Arabidopsis thaliana is generally independent of LHP1 and PRC2 activity. *Genome biology* **18**, 69.